J. Fluid Mech. (2016), *vol.* 795, *pp.* 847–875. © Cambridge University Press 2016
doi:10.1017/jfm.2016.231

Magneto-gravitational convection in a vertical layer of ferrofluid in a uniform oblique magnetic field

Habibur Rahman[1,‡] **and Sergey A. Suslov**[1,†]

[1]Department of Mathematics, H38, Swinburne University of Technology, John Street, Hawthorn, Victoria 3122, Australia

(Received 30 September 2015; revised 25 February 2016; accepted 28 March 2016; first published online 22 April 2016)

The stability of base gravitational convection in a layer of ferrofluid confined between two vertical wide and tall non-magnetic plates, heated from one side, cooled from the other and placed in a uniform oblique external magnetic field is studied. Two distinct mechanisms, thermo-gravitational and thermo-magnetic, are found to be responsible for the appearance of various stationary and wave-like instability modes. The characteristics of all instability modes are investigated as functions of the orientation angles of the applied magnetic field and its magnitude for various values of magnetic parameters when both the thermo-magnetic and gravitational buoyancy mechanisms are active. The original three-dimensional problem is cast in an equivalent two-dimensional form using generalised Squire's transformations, which significantly reduces a computational cost. Subsequently, full three-dimensional instability patterns are recovered using the inverse Squire's transformation, and the optimal field and pattern orientations are determined.

Key words: bifurcation, magnetic fluids, magneto convection

1. Introduction

Ferrofluids are non-conducting nanofluids containing solid single-domain ferromagnetic (e.g. magnetite, cobalt) nanoparticles with an average size of 10 nm suspended in an organic (e.g. kerosene, transformer oil) carrier or water (e.g. Charles 2002). The application of a magnetic field leads to a magnetisation of the solid phase that depends on the temperature (Curie effect). Because of their small size, the particles are assumed to be uniformly distributed in the bulk of a carrier fluid by their Brownian motion. Thus, at the macro scale, the magnetisation of individual particles is seen as the effective magnetisation of the fluid itself. As the temperature of the fluid increases, such bulk fluid magnetisation decreases due to the thermal expansion of a carrier fluid that reduces the effective concentration of magnetic particles and due to the disorientation of magnetic moments of individual particles by Brownian

† Email address for correspondence: ssuslov@swin.edu.au
‡ Present address: Department of Mathematics, Khulna University of Engingeering & Technology, Khulna 9203, Bangladesh.

motion (Rosensweig 1985; Bashtovoy, Berkovsky & Vislovich 1988). As a result, the so-called ponderomotive Kelvin force arises that drives the stronger magnetised colder fluid to the regions with a stronger magnetic field. Such a motion is referred to as magnetoconvection.

A pure magnetoconvection flow in a differentially heated ferrofluid layer placed in an oblique magnetic field was considered in Rahman & Suslov (2015). The prototype applications justifying such an investigation deal with flows that arise in situations where the gravitational buoyancy-driven convection is impossible, for example, in congested spaces of microelectronic devices or in microgravity conditions (Blums, Maiorov & Tsebers 1989; Odenbach 1995, 2002). It is known that the intensity of gravitational convection increases with the value of the Grashof number (e.g. Gershuni, Zhukhovitsky & Nepomniaschy 1989), which is proportional to the product of the gravity and the cube of the characteristic size of the domain filled with a fluid. Therefore the value of the Grashof number tends to 0 in outer space and in microelectronics applications. At the same time the magnetic Grashof number controlling magnetoconvection is independent of gravity and is proportional to only a square of the characteristic domain size. Thus magnetoconvection can be induced in a gravity-free environment, and it is easier to initiate in congested spaces than buoyancy-driven convection enabling the perspective use of magneto-convective flows for heat removal (Mukhopadhyay *et al.* 2005).

It is typical to model ferrofluids as single-component isotropic liquids with average transport properties that are close to those of a pure carrier fluid. However, such a simplified treatment can only be adopted if sufficient care is taken in determining the validity limits of such an approximation. The compositional inhomogeneity of a ferrofluid can in certain conditions lead to spatial dehomogenisation of the fluid invalidating simple constitutive models used for its description (Blums *et al.* 1989; Pshenichnikov & Ivanov 2012; Sprenger *et al.* 2015). The calibration and validation of such models must rely heavily on the results of experimental observations, which are quite rare to this day. There are objective reasons for that. Unfortunately, it is virtually impossible to conduct such experiments in environments directly corresponding to the potential working conditions of ferrofluids: direct flow observations in microelectronic devices are impossible due to the microscopic size of flow domains and the experimental studies on board space stations are prohibitively expensive. Therefore the majority of experimental ferrofluid flow investigations are conducted in ground-based experiments in finite-size (of the order of a few centimetres) non-magnetic containers (Bozhko & Putin 2003; Zablotsky, Mezulis & Blums 2009) shaped similarly to those found in potential applications (a rectangular geometry is common). However, this creates another serious problem on the way of the analysis. The magnetic field lines necessarily curve near the non-magnetic walls of the container that separate ferromagnetic medium from surroundings (the magnetic field is ‘sucked into’ a ferrofluid layer through its edges). Experiments reported in Suslov *et al.* (2010, 2012) show that the influence of such edge effects can extend far into the ferrofluid layer, so that they cannot be fully ignored.

A similar strong influence of the edge effects could be expected in free-surface ferrofluid layers of finite extent. Experiments and computations of Gollwitzer *et al.* (2009) performed in a small container confirm this. However, experimental photographs presented, for example, in Reimann *et al.* (2005), Groh *et al.* (2007) indicate that the magnetically forced periodic free-surface deformation patterns observed in the central part of a wide container appear to extend almost to its physical boundaries, thus downplaying the importance of the edge effects. The plausible

explanation of this drastic difference between free-surface and magnetoconvection experiments is that in the former case the focussing of a magnetic field under the curved fluid surface leads to a comparable or even stronger distortion of the applied field than that caused by the refraction of the magnetic field at the edges. In contrast, in fully a enclosed magnetoconvection system the deformation of the fluid surface is precluded so that the edge effects continue to play a dominant field-distorting role far away from the boundaries of a container. This is also supported by an experimental fact that even a slight deformation of the solid plate covering the fluid in wide-layer experiments of Suslov *et al.* (2012) caused by touching it with a (non-magnetic) thermometer led to a visible change of the local convection pattern that overpowered the variations caused by the edge effects in the absence of the cover deformation.

Since the curvature of magnetic field lines depends strongly on minor random imperfections of the experimental set-up and cannot be rendered easily to the analysis. To make progress in understanding physical processes taking place in ferrofluid convection in the gravity-free environment a compromise treatment was suggested by Rahman & Suslov (2015). Instead of simulating the flows in a finite ferrofluid layer and the distorted non-uniform magnetic field around it, which could only be done numerically for a limited set of governing parameters, the authors suggested to consider an infinite fluid layer subjected to an oblique magnetic field mimicking the magnetic field distortion in the near-edge regions of an experimental set-up.

The introduction of gravity expands the set of the governing parameters and, as will be evidenced by the reported stability results, leads to qualitatively different instabilities than those observed in a gravity-free setting. The analysis of various types of instabilities caused by the interaction of magnetic Kelvin and gravitational buoyancy forces is the major emphasis of this study. The other important aspect first reported in Rahman & Suslov (2015), which we will continue studying here, is the symmetry-breaking effect caused by the nonlinear variation of fluid magnetisation across the layer. The stability of a non-isothermal flow in a vertical layer of ordinary fluid is one of the classical problems of natural convection (Gershuni & Zhukhovitsky 1953; Batchelor 1954). It is known that for a class of large-Prandtl-number fluids to which kerosene- and transformer-oil-based ferrofluids belong to, the instability in this configuration occurs in the form of two waves counter-propagating along the direction of the gravity (Kirdyashkin, Leont'ev & Mukhina 1971). On the other hand the most dangerous instability mode detected in a normal magnetic field in the small gravity limit consists of stationary rolls with the axes parallel to the direction of the gravity (Suslov 2008). At the same time it has been shown in Rahman & Suslov (2015) that the oblique magnetic field tends to align the axes of the rolls with its in-layer component. Therefore it remains to be seen what exactly pattern orientation will result when an oblique magnetic field and the gravity act simultaneously. The study of such combined influences is what distinguishes the current investigation from previous research reported, for example, in Finlayson (1970), Bozhko & Putin (1991), Shliomis & Smorodin (2002), Hennenberg *et al.* (2006), Suslov (2008), Suslov *et al.* (2012) and references therein.

Prior to proceeding with the detailed mathematical formulation and the discussion of the governing parameters in § 2 we note that the considered physical problem is inherently three-dimensional. Yet, quite remarkably, we have been able to reduce the stability equations derived in § 3 to an equivalent two-dimensional formulation that enabled us to produce comprehensive stability results reported in § 4 without prohibitively expensive computations. The overall conclusions are given in § 5.

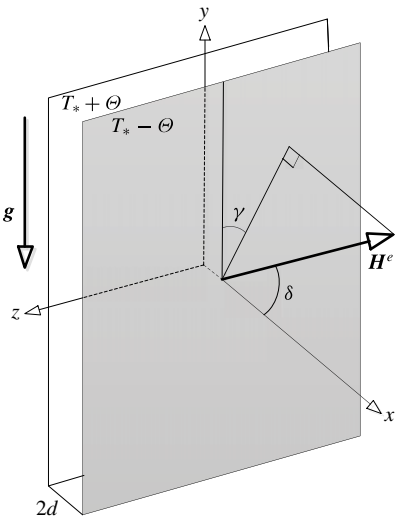

FIGURE 1. Sketch of the problem geometry. The vector of external magnetic field, $\boldsymbol{H}^e$ forms angles δ and γ with the coordinate axes.

2. Problem formulation and governing equations

Consider a layer of a ferromagnetic fluid that fills a gap between two infinitely long and wide parallel vertical non-magnetic plates as shown in figure 1. The plates are maintained at constant different temperatures $T_* \pm \Theta$. The right-hand system of coordinates (x, y, z) with the origin in the mid-plane of the layer is introduced in such a way that the plates are located at $x = \pm d$ and the y and z axes are parallel to the plates. The gravity $\boldsymbol{g} = (0, -g, 0)$ acts vertically down along the plates. An oblique external uniform magnetic field $\boldsymbol{H}^e = (H^e_x, H^e_y, H^e_z)$ such that $|\boldsymbol{H}^e| = H^e$ and

$$H^e_x = H^e \cos\delta, \quad H^e_y = H^e \sin\delta \cos\gamma, \quad H^e_z = H^e \sin\delta \sin\gamma, \tag{2.1a–c}$$

where δ and γ are the field inclination and orientation angles, respectively, is applied to the layer. This field induces a magnetic field $\boldsymbol{H}$, $|\boldsymbol{H}| = H$ within the layer. The magnetic field causes fluid magnetisation $\boldsymbol{M}$, $|\boldsymbol{M}| = M$, which is assumed to be co-directed with the internal magnetic field: $\boldsymbol{M} = \chi_* \boldsymbol{H}$, where χ_* is the integral magnetic susceptibility of the fluid. Assuming that the temperature difference 2Θ between the walls is sufficiently small we adopt the Boussinesq approximation of the continuity, Navier–Stokes, and thermal energy equations that are complemented with the Maxwell equations for the magnetic field written in the magneto-static form due to the negligible electrical conductivity of ferrofluids (Rosensweig 1985). As discussed in Suslov (2008), the non-dimensional governing equations for velocity $\boldsymbol{v} = (u, v, w)$, temperature variation θ, pressure P, magnetic field $\boldsymbol{H}$ and magnetisation $\boldsymbol{M}$ read

$$\nabla \cdot \boldsymbol{v} = 0, \tag{2.2}$$

$$\frac{\partial \boldsymbol{v}}{\partial t} + \boldsymbol{v} \cdot \nabla \boldsymbol{v} = -\nabla P + \nabla^2 \boldsymbol{v} - Gr\,\theta \boldsymbol{e}_g - Gr_m \theta \nabla H, \tag{2.3}$$

$$\frac{\partial \theta}{\partial t} + \boldsymbol{v} \cdot \nabla \theta = \frac{1}{Pr} \nabla^2 \theta, \tag{2.4}$$

$$\boldsymbol{\nabla}\times\boldsymbol{H}=\boldsymbol{0}, \tag{2.5}$$

$$(1+\chi)(\boldsymbol{\nabla}\cdot\boldsymbol{H}-\boldsymbol{\nabla}\theta\cdot\boldsymbol{e})+\frac{(\chi_*-\chi)N-(1+\chi)\theta}{H}(\boldsymbol{\nabla}\cdot\boldsymbol{H}-\boldsymbol{\nabla}H\cdot\boldsymbol{e})=0, \tag{2.6}$$

$$\boldsymbol{M}=[\chi H+(\chi_*-\chi)N-(1+\chi)\theta]\boldsymbol{e} \tag{2.7}$$

with the boundary conditions

$$[((1+\chi)(H\pm1)+(\chi_*-\chi)N)\boldsymbol{e}-\boldsymbol{H}^e]\cdot\boldsymbol{n}=0, \tag{2.8}$$

$$\boldsymbol{v}=\boldsymbol{0},\quad \theta=\mp1\quad \text{at } x=\pm1, \tag{2.9a,b}$$

where $\boldsymbol{e}=(e_1,e_2,e_3)\equiv\boldsymbol{H}/H$.

The dimensionless groups appearing in the problem are

$$Gr=\frac{\rho_*^2\beta_*\Theta g d^3}{\eta_*^2},\quad Gr_m=\frac{\mu_0\rho_*K_*^2\Theta^2d^2}{\eta_*^2(1+\chi)},\quad Pr=\frac{\eta_*}{\rho_*\kappa_*},\quad N=\frac{H_*(1+\chi)}{K_*\Theta}, \tag{2.10a–d}$$

where ρ_* is the density, η_* is the dynamic viscosity, β_* is the coefficient of thermal expansion, κ_* is the thermal diffusivity, $\chi=\partial M/\partial H|_{(H_*,T_*)}$ is the differential magnetic susceptibility, $K_*=-\partial M/\partial T|_{(H_*,T_*)}$ is the pyromagnetic coefficient of the fluid and $\mu_0=4\pi\times10^{-7}$ H m^{-1} is the magnetic constant. The subscript $*$ denotes the values of the fluid properties evaluated at the reference temperature T_* and magnetic field H_*. The thermo-gravitational and magnetic Grashof numbers Gr and Gr_m characterise the importance of buoyancy and magnetic forces, respectively, the Prandtl number Pr is the ratio of viscous and thermal diffusion transports, and parameter N describes the strength of the magnetic field at the reference location relative to the variation of fluid magnetisation due to thermal effects. Unless specified otherwise, we fix the value of Prandtl number to $Pr=55$ and choose $\chi=\chi_*=3$ (which corresponds to a linear magnetisation regime) as in experiments of Bozhko *et al.* (2013). We also consider smaller values of $\chi=1.5$ and 0.5 and of $\chi=2.5$ and 1.5 that correspond to the near-saturation magnetic regimes, see Rahman & Suslov (2015).

The thermo-magnetic sensitivity of ferrofluids is characterised by the pyromagnetic coefficient K_* (see figure 2*b* in Rahman & Suslov (2015)). Non-dimensionally, this is accounted for by the values of the parameter N defined in (2.10) or, equivalently, by the magnitude of the non-dimensional applied magnetic field H^e, see figure 2(*d*) in Rahman & Suslov (2015). Since both N and H^e are inversely proportional to K_*, more thermomagnetically sensitive fluids are characterised by the smaller values of these parameters. To compare the behaviour of fluids with different thermo-magnetic sensitivities the results are reported for the representative magnitudes of the non-dimensional external magnetic field $H^e=100$ and $H^e=10$. The first value corresponds to the experimental conditions of Suslov *et al.* (2010, 2012), Bozhko *et al.* (2013) and Sidorov (2016), while the second is chosen consistently with Rahman & Suslov (2015) to highlight the effects caused by the nonlinearity of magnetic field within the fluid layer.

Our computations and recent experimental studies (Sidorov 2016) demonstrate a rapid stabilisation of ferrofluid flows in the considered geometry as the applied field deviates from normal. For this reason only relatively small field inclination angles $0^\circ\leqslant\delta\leqslant15^\circ$ will be considered here. In contrast, all possible field orientations $0^\circ\leqslant\gamma\leqslant180^\circ$ will be inspected. No a priori limitations will be imposed on the values of Grashof numbers Gr and Gr_m.

3. Basic flow and linearised stability equations

As shown in Suslov (2008) and Rahman & Suslov (2015), (2.2)–(2.9) admit steady solutions

$$\theta_0 = -x, \quad v_0 = \frac{Gr}{6}(x^3 - x), \quad P_0 = Gr_m \int_0^x \widetilde{x} e_{10} D H_{x0}\, \mathrm{d}\widetilde{x} + C, \tag{3.1a–c}$$

$$H_{y0}(x) = H_y^e, \quad H_{z0}(x) = H_z^e, \tag{3.2a,b}$$

where $D \equiv \mathrm{d}/\mathrm{d}x$, C is an arbitrary constant and

$$\boldsymbol{e}_0(x) \equiv (e_{10}(x), e_{20}(x), e_{30}(x)) = \left(\frac{H_{x0}}{H_0}, \frac{H_y^e}{H_0}, \frac{H_z^e}{H_0}\right) \tag{3.3}$$

is the unit vector in the direction of the magnetic field. The nonlinear variation of an oblique magnetic field across the fluid layer cannot be given in a closed form and has to be computed numerically by solving the equation

$$((1+\chi)(H_0 - \theta_0) + (\chi_* - \chi)N)H_{x0} = H_x^e H_0, \tag{3.4}$$

where $H_0 \equiv \sqrt{H_{x0}^2 + H_{y0}^2 + H_{z0}^2}$. Once the magnetic field within the layer is determined the unperturbed fluid magnetisation is computed using

$$M_0 \equiv \sqrt{M_{x0}^2 + M_{y0}^2 + M_{z0}^2} = \chi H_0 + (\chi_* - \chi)N - (1+\chi)\theta_0. \tag{3.5}$$

The nonlinearity of the function $H_{x0}(x)$ that occurs in ferrofluids with large magnetic susceptibilities has been shown to play a symmetry-breaking role, which in turn leads to significant qualitative and quantitative changes in stability characteristics of the considered flow. In particular, the appearance of wave-like instability patterns that do not exist in a normal field have been linked to the curvature of magnetic field lines within a ferrofluid layer (Rahman & Suslov 2015). Of the main interest in the current study is how such a thermomagnetically induced symmetry breaking interacts with yet another feature of a realistic physical set-up, the loss of the spatial degeneracy due to the introduction of the preferred direction along the gravity vector.

To investigate a linear stability of the basic state with respect to infinitesimal y and z-periodic disturbances the perturbed quantities are written in a normal form

$$\begin{aligned}(\boldsymbol{v}, P, \theta, \boldsymbol{H}, H, \boldsymbol{M}, M) &= (\boldsymbol{v}_0, P_0, \theta_0, \boldsymbol{H}_0, H_0, \boldsymbol{M}_0, M_0) \\ &+ [(\boldsymbol{v}_1(x), P_1(x), \theta_1(x), \boldsymbol{H}_1(x), H_1(x), \boldsymbol{M}_1(x), M_1(x))\mathrm{e}^{\sigma t + \mathrm{i}(\alpha y + \beta z)} + \text{c.c.}],\end{aligned} \tag{3.6}$$

where $\sigma = \sigma^R + \mathrm{i}\sigma^I$ is the complex amplification rate, α and β are real wavenumbers in the y and z directions, respectively and c.c. denotes the complex conjugate of the expression in brackets. Upon introducing the magnetic potential $\phi_1(x)\mathrm{e}^{\sigma t + \mathrm{i}(\alpha y + \beta z)}$ such that $\boldsymbol{H}_1(x) = (D\phi_1, \mathrm{i}\alpha\phi_1, \mathrm{i}\beta\phi_1)$ and applying Squire's transformations

$$\left.\begin{gathered}(x, y, z) = (\widetilde{x}, \widetilde{y}, \widetilde{z}), \quad \theta_0 = \widetilde{\theta}_0, \quad H_{x0} = \widetilde{H}_{x0}, \quad H_0 = \widetilde{H}_0, \quad \sigma = \widetilde{\sigma}, \\ \alpha^2 + \beta^2 = \widetilde{\alpha}^2, \quad \beta = \widetilde{\beta}, \quad u_1 = \widetilde{u}, \quad \alpha v_1 + \beta w_1 = \widetilde{\alpha}\widetilde{v}, \quad w_1 = \widetilde{w}, \quad \theta_1 = \widetilde{\theta}, \\ P_1 = \widetilde{P}, \quad \phi_1 = \widetilde{\phi}, \quad \alpha Gr = \widetilde{\alpha}\widetilde{Gr}, \quad Gr_m = \widetilde{Gr}_m, \quad Pr = \widetilde{Pr}, \quad N = \widetilde{N}, \\ \chi = \widetilde{\chi}, \quad \chi_* = \widetilde{\chi}_*,\end{gathered}\right\} \tag{3.7}$$

$$e_{10} = \widetilde{e}_{10}, \quad \alpha e_{20} + \beta e_{30} = \widetilde{\alpha}\widetilde{e}_{20} \tag{3.8a,b}$$

the linearised perturbation equations are written as

$$0 = D\widetilde{u} + \mathrm{i}\widetilde{\alpha}\widetilde{v}, \tag{3.9}$$

$$\widetilde{\sigma}\widetilde{u} + (\widetilde{\alpha}^2 + \mathrm{i}\widetilde{\alpha}\widetilde{v}_0 - D^2)\widetilde{u} + D\widetilde{P} + \widetilde{e}_{10}\widetilde{Gr}_m D\widetilde{H}_{x0}\widetilde{\theta} + \widetilde{Gr}_m\widetilde{\theta}_0\widetilde{e}_{10}D^2\widetilde{\phi} + \widetilde{Gr}_m\widetilde{\theta}_0\left[\mathrm{i}\widetilde{\alpha}\widetilde{e}_{20} + (1-\widetilde{e}_{10}^2)\frac{D\widetilde{H}_{x0}}{\widetilde{H}_0}\right]D\widetilde{\phi} - \mathrm{i}\widetilde{\alpha}\widetilde{Gr}_m\widetilde{\theta}_0\widetilde{e}_{10}\widetilde{e}_{20}\frac{D\widetilde{H}_{x0}}{\widetilde{H}_0}\widetilde{\phi} = 0, \tag{3.10}$$

$$\widetilde{\sigma}\widetilde{v} + D\widetilde{v}_0\widetilde{u} + (\widetilde{\alpha}^2 + \mathrm{i}\widetilde{\alpha}\widetilde{v}_0 - D^2)\widetilde{v} + \mathrm{i}\widetilde{\alpha}\widetilde{P} - \widetilde{Gr}\widetilde{\theta} + \widetilde{\alpha}\widetilde{Gr}_m\widetilde{\theta}_0(\mathrm{i}\widetilde{e}_{10}D\widetilde{\phi} - \widetilde{\alpha}\widetilde{e}_{20}\widetilde{\phi}) = 0, \tag{3.11}$$

$$\widetilde{\sigma}\widetilde{w} + (\widetilde{\alpha}^2 + \mathrm{i}\widetilde{\alpha}\widetilde{v}_0 - D^2)\widetilde{w} + \mathrm{i}\widetilde{\beta}\widetilde{P} + \widetilde{\beta}\widetilde{Gr}_m\widetilde{\theta}_0(\mathrm{i}\widetilde{e}_{10}D\widetilde{\phi} - \widetilde{\alpha}\widetilde{e}_{20}\widetilde{\phi}) = 0, \tag{3.12}$$

$$\widetilde{\sigma}\widetilde{\theta} + D\widetilde{\theta}_0\widetilde{u} + \left(\frac{\widetilde{\alpha}^2 - D^2}{\widetilde{Pr}} + \mathrm{i}\widetilde{\alpha}\widetilde{v}_0\right)\widetilde{\theta} = 0, \tag{3.13}$$

$$\begin{aligned} 0 \;=\; & (D^2 - \widetilde{\alpha}^2)\widetilde{\phi} + (1-\widetilde{e}_{10}^2)\left(\frac{\widetilde{\chi}_* - \widetilde{\chi}}{1+\widetilde{\chi}}\widetilde{N} - \widetilde{\theta}_0\right)\frac{D^2\widetilde{\phi}}{\widetilde{H}_0} - \left[(1-\widetilde{e}_{10}^2)D\widetilde{\theta}_0 \right. \\ & \left. + \widetilde{e}_{10}\left(\frac{\widetilde{\chi}_* - \widetilde{\chi}}{1+\widetilde{\chi}}\widetilde{N} - \widetilde{\theta}_0\right)\left(2\mathrm{i}\widetilde{\alpha}\widetilde{e}_{20} + 3(1-\widetilde{e}_{10}^2)\frac{D\widetilde{H}_{x0}}{\widetilde{H}_0}\right)\right]\frac{D\widetilde{\phi}}{\widetilde{H}_0} \\ & - \left[\left(\frac{\widetilde{\chi}_* - \widetilde{\chi}}{1+\widetilde{\chi}}\widetilde{N} - \widetilde{\theta}_0\right)\left(\widetilde{\alpha}^2(1-\widetilde{e}_{20}^2) + \mathrm{i}\widetilde{\alpha}\widetilde{e}_{20}(1-3\widetilde{e}_{10}^2)\frac{D\widetilde{H}_{x0}}{\widetilde{H}_0}\right)\right. \\ & \left. - \mathrm{i}\widetilde{\alpha}\widetilde{e}_{20}\widetilde{e}_{10}D\widetilde{\theta}_0\right]\frac{\widetilde{\phi}}{\widetilde{H}_0} - \left(\mathrm{i}\widetilde{\alpha}\widetilde{e}_{20} + (1-\widetilde{e}_{10}^2)\frac{D\widetilde{H}_{x0}}{\widetilde{H}_0}\right)\widetilde{\theta} - \widetilde{e}_{10}D\widetilde{\theta}, \end{aligned} \tag{3.14}$$

with the boundary conditions

$$\left(1 + \widetilde{\chi} + (1-\widetilde{e}_{10}^2)\frac{(\widetilde{\chi}_* - \widetilde{\chi})\widetilde{N} \pm (1+\widetilde{\chi})}{\widetilde{H}_0}\right)D\widetilde{\phi} \pm |\widetilde{\alpha}|\widetilde{\phi} - \mathrm{i}\widetilde{\alpha}\widetilde{e}_{10}\widetilde{e}_{20}\frac{(\widetilde{\chi}_* - \widetilde{\chi})\widetilde{N} \pm (1+\widetilde{\chi})}{\widetilde{H}_0}\widetilde{\phi} = 0, \tag{3.15}$$

$$\widetilde{u} = \widetilde{v} = \widetilde{w} = \widetilde{\theta} = 0 \quad \text{at } \widetilde{x} = \pm 1. \tag{3.16}$$

Only (3.12) contains $\widetilde{w}$ and β explicitly. Therefore this equation can be split from the rest of the transformed system and, if necessary, solved afterwards. The remaining equations form an equivalent two-dimensional problem that can be formally obtained by setting $w = \beta = 0$, that is by assuming the two-dimensionality of the perturbation field and its periodicity in the y direction. This enables one to significantly reduce the computational cost of stability calculations. However, even if β and w are set to 0 the external applied magnetic field (2.1) still remains three-dimensional in the above Squire-transformed linearised equations and thus the field inclination and orientation angles δ and γ still act as independent control parameters entering the problem via the expressions for $\widetilde{e}_{20}$. Note that in contrast to the analysis of Rahman & Suslov (2015), where the direction of the y axis was linked to that of the in-layer component of the applied magnetic field, here it is rigidly linked to the direction of the gravity while the orientation of the magnetic field is chosen independently. In general, the orientation of instability patterns in flows considered here is not known beforehand

and thus will have to be determined by applying the inverse Squire's transformation after the equivalent two-dimensional problem formulated above is solved. However, if as a result of solving the equivalent two-dimensional problem it is established that the instability occurs (i.e. $\widetilde{\sigma}^R$ monotonically increases from negative to positive values) as $\widetilde{Gr}$ increases while $\widetilde{Gr}_m$ remains fixed then a definite conclusion can be made about the orientation of the most amplified perturbation patterns without the necessity of inverting Squire's transformation in each computational run. Indeed, according to (3.7) while the value of the disturbance amplification rate is invariant with respect to Squire's transformation ($\sigma = \widetilde{\sigma}$) the value of Gr for the original three-dimensional problem is always equal to or larger than that of $\widetilde{Gr}$ for the equivalent two-dimensional problem:

$$Gr = \frac{\widetilde{\alpha}}{\alpha}\widetilde{Gr} = \frac{\sqrt{\alpha^2+\beta^2}}{\alpha}\widetilde{Gr} \geqslant \widetilde{Gr}. \tag{3.17}$$

This means that in this case instability indeed first sets in the form of two-dimensional y-periodic patterns that correspond to $\beta = 0$, the full original and Squire-transformed problems have identical solutions and Squire's theorem holds. This fact will be used extensively in the discussion of numerical results in § 4.

Note that it follows from the problem geometry and Squire's transformation (3.7) that

$$\frac{\alpha H_y^e + \beta H_z^e}{H^e} = \alpha \sin\delta\cos\gamma + \beta\sin\delta\sin\gamma = \widetilde{\alpha}\frac{\widetilde{H}_y}{H^e} = \widetilde{\alpha}\sin\delta\cos\widetilde{\gamma}, \tag{3.18}$$

or, for an oblique field with $\delta \neq 0°$, $\alpha\cos\gamma + \beta\sin\gamma = \sqrt{\alpha^2+\beta^2}\cos\widetilde{\gamma}$. Then

$$\gamma = \tan^{-1}\frac{\beta}{\alpha} \pm \widetilde{\gamma}. \tag{3.19}$$

In particular, if $\beta = 0$ then $\gamma = \pm\widetilde{\gamma}$. However, when $\alpha = 0$ then $\gamma = 90° \pm \widetilde{\gamma}$. It is convenient to choose $\widetilde{\gamma}$ as an independent problem parameter characterising the magnetic field orientation keeping in mind its meaning given by (3.19).

To simplify the notation, in the subsequent sections we will use tilde to denote only the non-trivially transformed quantities $\widetilde{\alpha}$, $\widetilde{v}$, $\widetilde{Gr}$, $\widetilde{\gamma}$ and $\widetilde{e}_{20}$.

4. Flow stability characteristics

4.1. *Numerical procedure and comparison with selected previous numerical results*

The numerical code based on the pseudo-spectral Chebyshev collocation method (see Rahman & Suslov (2015) and references therein for details) that was used for solving (3.9)–(3.16) was tested against the known results. The critical values of $\widetilde{Gr} = 502.35$ and $\widetilde{\alpha} = 1.405$ were computed for a pure gravitational ($Gr_m = 0$) convection at Prandtl number $Pr = 0.71$. After multiplying by the corresponding scaling factors of 16 and 2, respectively, arising due to a different non-dimensionalisation they agree with results reported in Suslov & Paolucci (1995). The onset of gravitational convection is also computed for $Pr = 7$ and the set of critical values $(\widetilde{Gr}, \widetilde{\alpha}) = (491.78, 1.38)$ is obtained, which agrees closely with that presented in Belyaev & Smorodin (2010). The critical values $(Gr_m, \widetilde{\alpha}) = (1.387, 1.928)$ found for the magnetoconvection threshold ($\widetilde{Gr} = 0$) in a perpendicular ($\delta = 0°$) external magnetic field for $Pr = 130$ and $\chi = \chi_* = 4$ agree well with $(Gr_m, \widetilde{\alpha}) = (1.385, 1.95)$ computed from the corresponding data reported in Finlayson (1970).

4.2. *Stability characteristics of flows in a normal field*

The stability characteristics of a ferromagnetic fluid flow in a vertical differentially heated layer placed in a normal magnetic field have been investigated previously by Suslov (2008). However, there the author discussed only flow stability for a fluid with the specific Prandtl number $Pr = 130$ and in a linear magnetisation regime with $\chi = \chi_* = 5$. Subsequently, Belyaev & Smorodin (2010) reported results for a similar geometry, but for different values of Prandtl number and magnetic susceptibilities. The results reported in this section are chosen to make the subsequent discussion self-contained and to complement the data reported previously. In particular, the aspects related to the $x \to -x$ symmetry-breaking effect of a nonlinear cross-layer variation of the fluid's magnetisation have not been discussed in literature before and will be addressed here. Unless specified otherwise the numerical results will be presented for $Pr = 55$, which corresponds to the fluid used in experiments of Bozhko *et al.* (2013).

As reported in Suslov (2008), three main types of instability patterns corresponding to magnetic, thermo-gravitational and magneto-gravitational convection have been found to exist in a normal magnetic field in the considered geometry. Similar to Rayleigh–Bénard and Rayleigh–Marangoni convection, pure magnetoconvection patterns appearing in a normal magnetic field possess full planar (y, z) symmetry (Finlayson 1970). The vertical gravity acting along the fluid layer breaks this symmetry leading to the appearance of preferential thermo-gravitational convection patterns that are periodic in the vertical (y) direction, and preferential magnetoconvection patterns, which are periodic in the horizontal z direction. The interaction of the two convection mechanisms may lead to the appearance of three-dimensional patterns that are periodic in both y and z directions. The typical leading eigenvalues (the amplification rate $\sigma^R(\widetilde{\alpha})$ and the frequency $\sigma^I(\widetilde{\alpha})$) are shown in figure 2. In the first case ($Gr_m \to 0$) one maximum of the disturbance amplification rate σ^R exists for a pair of leading complex conjugate eigenvalues, see figure 2(*a*,*d*). This indicates the existence of two counter-propagating thermal waves (see, for example, Kirdyashkin *et al.* (1971), Gershuni *et al.* (1989) and references therein for a historical overview) corresponding to the thermo-gravitational convection instability. The two waves caused by the gravitational buoyancy propagate up and down near the hot and cold walls, respectively. Since they have equal growth rates they are expected to form fully symmetric perturbation patterns illustrated in figure 3. If $Gr_m = 0$ such patterns are fully independent of the characteristics of the applied magnetic field. As discussed in Suslov (2008), their qualitative structure remains unchanged for moderate non-zero values of Gr_m, however their quantitative characteristics do depend on the magnetic Grashof number. In the subsequent text we will refer to this instability, which is caused mainly by thermal waves, as the Type I instability.

In the second limiting case ($\widetilde{Gr} \to 0$) one maximum of the disturbance amplification rate σ^R is also found but now the leading eigenvalues are real, see figure 2(*b*,*e*). This situation corresponds to stationary magnetoconvection patterns illustrated in figure 4. It is caused by the action of the ponderomotive Kelvin force. Such a force leads to the so-called magnetic buoyancy when cooler and thus stronger magnetised fluid particles are driven toward the hotter regions with a stronger magnetic field and *vice versa*. In a vertical fluid layer heated and cooled from the sides the magnetic buoyancy force acts in the horizontal direction across the fluid layer. For brevity the instability caused by the magnetic buoyancy will be referred to as the Type II instability. The perturbation cells in this case are centrally located and symmetric with respect to the mid-plane of the layer. Because of this the disturbances remain stationary as the basic flow velocity at the centre of the layer is zero. As will be shown in the subsequent sections, this

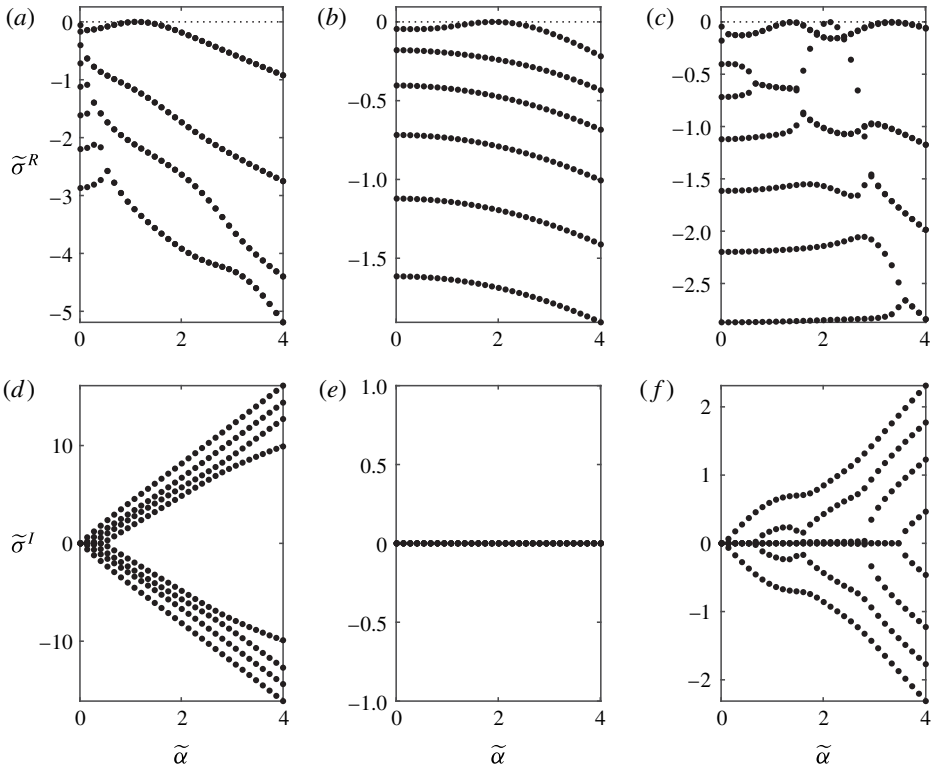

FIGURE 2. Leading disturbance temporal amplification rates $\widetilde{\sigma}^R$ (*a–c*) and frequencies $\widetilde{\sigma}^I$ (*d–f*) as functions of the transformed wavenumber $\widetilde{\alpha}$ for (*a*,*d*) $(\widetilde{Gr}_m, \widetilde{Gr}) = (0, 65.335)$ (onset of thermo-gravitational convection), (*b*,*e*) $(\widetilde{Gr}_m, \widetilde{Gr}) = (3.241, 0)$ (onset of stationary magnetoconvection) and (*c*,*f*) $(\widetilde{Gr}_m, \widetilde{Gr}) = (41.03, 11.26)$ at $\delta = 0°$, $\widetilde{\chi} = \widetilde{\chi}_* = 3$ and $\widetilde{Pr} = 55$. In plot (*c*), the left, right and middle local $\widetilde{\sigma}^R$ maxima correspond to small- and large-wavenumber waves and a stationary roll pattern, respectively.

symmetry breaks when the applied magnetic field is not strictly normal to the layer, which causes the drift of magnetoconvection patterns. The Type II instability in the absence of gravity has been discussed in detail in Rahman & Suslov (2015). Thus in the present article we will focus mostly on the influence that the gravity has on the Type II instability rather than on its physical nature described elsewhere.

In the third case ($\widetilde{Gr} \neq 0$, $Gr_m \neq 0$), up to three maxima of the disturbance amplification rate σ^R can exist (see figure 2*c*), of which the left- and right-most maxima correspond to small- and large-wavenumber waves while the middle one corresponds to a stationary magnetoconvection pattern. The comparison of figures 3 and 5, and 4 and 6 demonstrates that the perturbation fields are similar in these cases, so that the left and middle maxima of the $\sigma(\widetilde{\alpha})$ curves correspond to the Type I and Type II instabilities, respectively (see also discussion in Suslov (2008)). While always present for $Gr_m \neq 0$, the magnetic effects do not change the thermal waves significantly in normal magnetic field.

Figure 6 demonstrates that in the presence of gravity the magnetically driven Type II instability detected for non-zero $\widetilde{Gr}$ still takes the form of centrally located cells, which however are now sheared by the basic flow velocity with a cubic

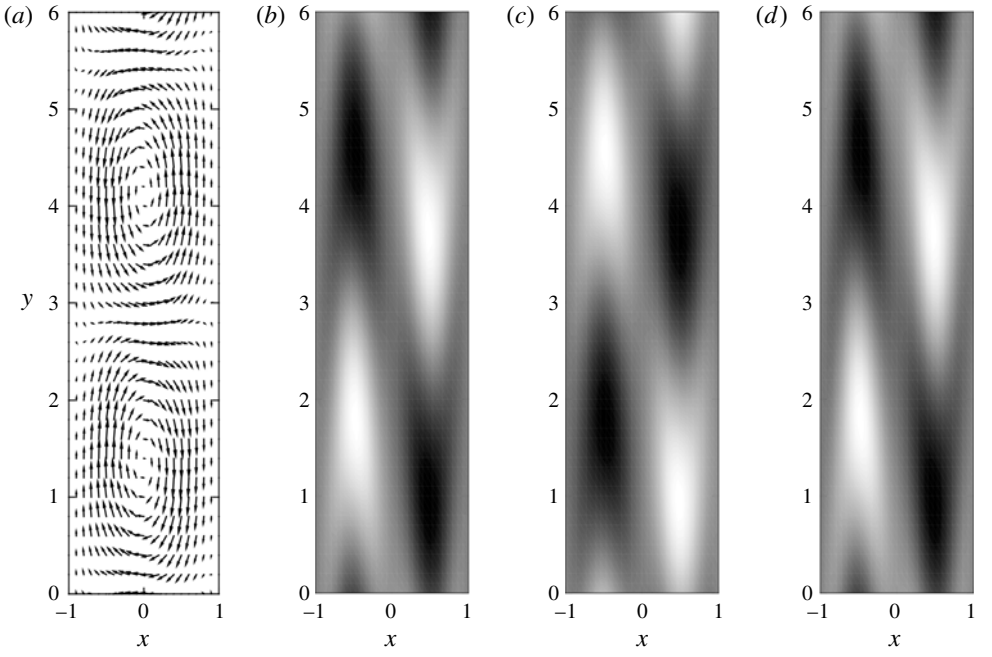

FIGURE 3. Instantaneous perturbation fields of (*a*) the fluid velocity $\boldsymbol{v}_1$, (*b*) the temperature θ_1, (*c*) the magnetisation M_1 and (*d*) the magnetic field H_1 for thermo-gravitational convection in a normal field ($\delta = 0°$) for $H^e = 100$, $\chi = \chi_* = 3$ and at the critical point for $Gr_m = 0$, $\widetilde{Gr} = 65.335$ and $\widetilde{\alpha} = 1.127$.

profile (3.1), where fluid rises near the hot left wall and sinks near the cold right wall. The short-wave instability corresponding to the right maximum of the leading $\sigma(\widetilde{\alpha})$ branch in figure 2(*c*) will be referred to as the Type III instability. The corresponding perturbation fields appear to be similar to thermo-gravitational waves, compare figures 3 and 7, however their exact nature cannot be determined via a parametric continuation from either of the two limiting cases mentioned above (Suslov *et al.* 2012).

As mentioned previously, in the absence of a magnetic field (or, equivalently, when $Gr_m = 0$) the problem under consideration possesses symmetry that results in thermo-gravitational instability in the form of two thermal waves with equal linear growth rates propagating with equal speeds in the opposite directions. Computational results presented previously in Suslov (2008) indicated that such a symmetry is preserved when a normal magnetic field is applied to a fluid layer. Yet our current computational data given in table 1 demonstrate that even the normal field is capable of breaking the symmetry between the two counter-propagating waves. This apparent discrepancy with the previous results is traced back to the form of the magnetisation equation (2.7) used in computations. In Suslov (2008) it was linearised by assuming small variations of the magnitude of a magnetic field so that a cross-layer symmetry of fluid magnetisation was enforced. Here we choose to perform calculations using (2.7) directly without simplifying it any further. Then for $\delta = 0°$ the magnetic potential equation (3.14) becomes

$$\left(D^2 - \frac{1+\chi_*}{1+\chi}\frac{\widetilde{\alpha}^2}{1-x/N}\right)\phi - D\theta = 0\,. \tag{4.1}$$

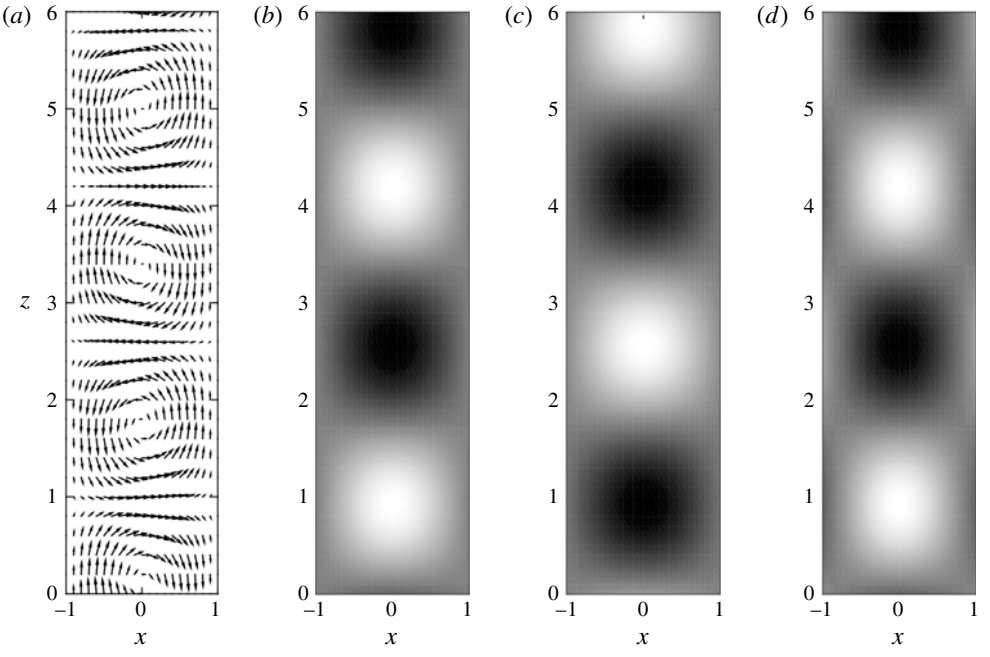

FIGURE 4. Same as figure 3 but for $Gr_m = 3.241$, $\widetilde{Gr} = 0$ and $\widetilde{\alpha} = 1.915$.

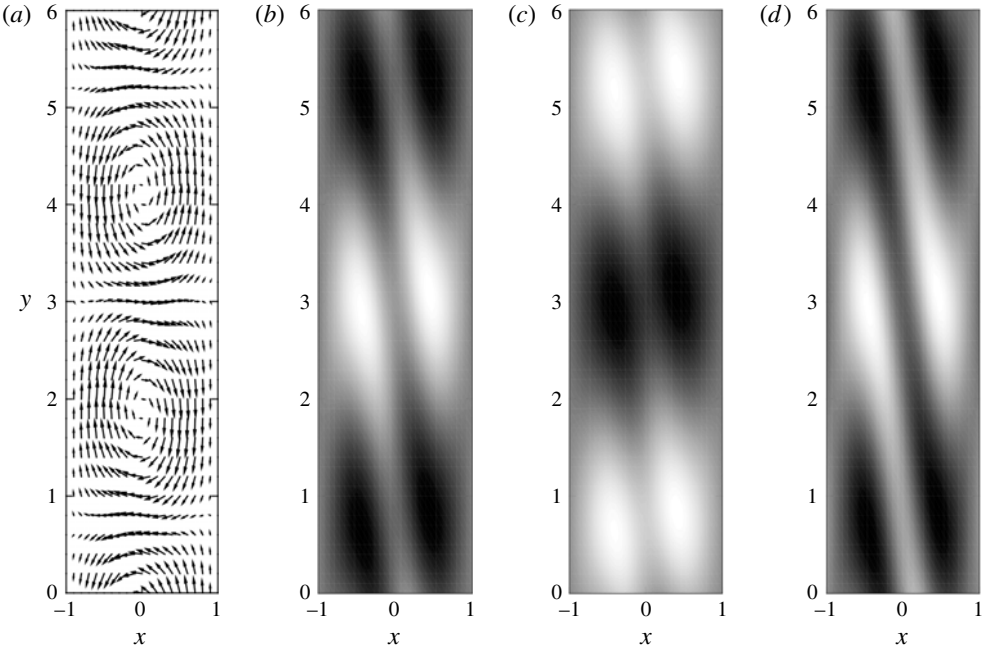

FIGURE 5. Same as figure 3 but for $Gr_m = 41.03$, $\widetilde{Gr} = 11.26$ and $\widetilde{\alpha} = 1.384$.

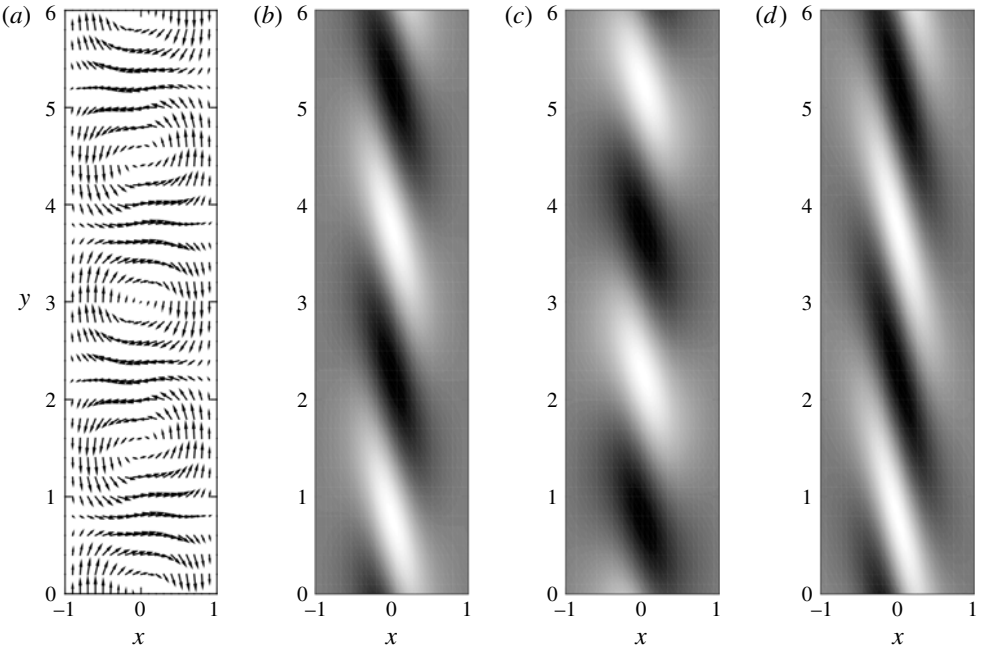

FIGURE 6. Same as figure 3 but for $Gr_m = 41.03$, $\widetilde{Gr} = 11.26$ and $\widetilde{\alpha} = 2.11$.

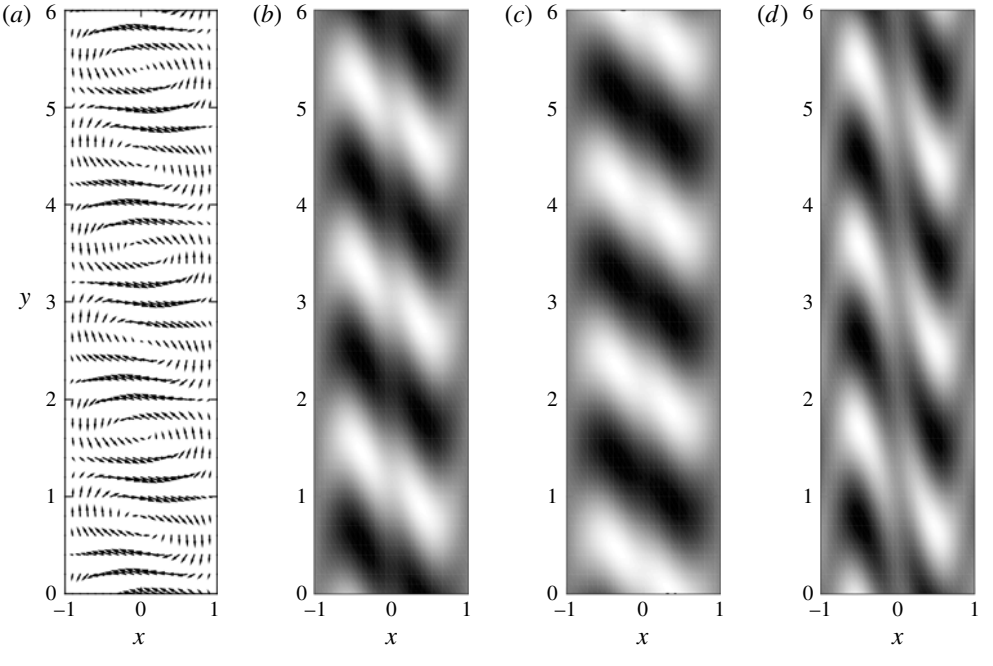

FIGURE 7. Same as figure 3 but for $Gr_m = 41.03$, $\widetilde{Gr} = 11.26$ and $\widetilde{\alpha} = 3.342$.

		Wave propagating downward			Wave propagating upward		
χ	χ_*	$\widetilde{\alpha}_c$	$\widetilde{Gr}_c$	$\widetilde{c}_c$	$\widetilde{\alpha}_c$	$\widetilde{Gr}_c$	$\widetilde{c}_c$
5	5	1.219	57.39	−3.655	1.215	57.60	3.670
3	5	1.240	54.88	−3.486	1.236	55.15	3.504
3	3	1.220	56.89	−3.622	1.218	57.01	3.631
1.5	2.5	1.239	54.58	−3.467	1.237	54.70	3.476
0.5	1.5	1.250	52.78	−3.347	1.248	52.86	3.353

TABLE 1. The critical values of Grashof number $\widetilde{Gr}$, wavenumber $\widetilde{\alpha}$ and disturbance wave speed $\widetilde{c} = -\sigma^I/\widetilde{\alpha}$ for the two leading waves of magneto-gravitational convection in a normal magnetic field ($\delta = 0°$) for $Gr_m = 15$, $H^e = 100$, $Pr = 55$ and various values of χ and χ_*.

It differs from (51) in Suslov (2008) due to the presence of the term $-x/N$ in the denominator. As has been discussed in Rahman & Suslov (2015), in typical applications this term is of the order of 10^{-2} or smaller and can be safely neglected if computational results are to be compared with experimental observations. However, one of our goals here is to investigate the symmetry-breaking effects, which this term contributes to. Therefore here we work with a full version of the magnetisation equation (2.7).

The representative computational results for $Gr_m = 15$ demonstrating the symmetry-breaking effect of a nonlinear magnetisation distribution are given in table 1. These data show that the basic flow becomes unstable with respect to the downward wave at slightly smaller values of $\widetilde{Gr}$. At their respective onsets the downward waves propagate with a slightly smaller wave speeds and have a slightly shorter wavelengths than their upward counterparts. This is in contrast to the completely symmetrical thermal waves observed at $Gr_m = 0$ and characterised by the critical values of $(\widetilde{Gr}, \widetilde{\alpha}, \widetilde{c}) = (65.34, 1.127, \pm 4.202)$ at $Pr = 55$. In addition to the symmetry-breaking effect of the fluid's magnetisation, the data in table 1 reveal that the application of a normal magnetic field always leads to the reduction of the critical value of the Grashof number. Thus we conclude that the normal magnetic field (or the normal component of the applied oblique magnetic field) plays a destabilising role. Somewhat counter-intuitively, the data also show that the basic flow of stronger magnetisable fluids with a larger differential magnetic susceptibility χ remains more stable indicating a subtle interplay between the fluid magnetisation on one hand and its ability to 'screen' the applied magnetic field on the other. The instability also is promoted as the fluid approaches magnetic saturation (when both χ and χ_* decrease and χ becomes smaller than χ_*).

4.3. *Wave-like instabilities in an oblique field*

In this section we will discuss in detail the characteristics of the Type I instability appearing in the form of two counter-propagating waves. The representative critical values similar to those given in table 1 for this instability observed in an oblique magnetic field are presented in table 2 for various field inclination angles. As follows from the data in these tables, the basic flow becomes more stable when the field inclination angle increases beyond $\delta = 5°$. The main (but not the only) reason for this stabilisation is the geometrical reduction of the normal component of the applied

		$\delta = 5°$			$\delta = 10°$			$\delta = 15°$		
χ	χ_*	$\widetilde{\alpha}_c$	$\widetilde{Gr}_c$	$\widetilde{c}_c$	$\widetilde{\alpha}_c$	$\widetilde{Gr}_c$	$\widetilde{c}_c$	$\widetilde{\alpha}_c$	$\widetilde{Gr}_c$	$\widetilde{c}_c$
					Wave propagating upward					
3	3	1.232	57.03	3.643	1.200	61.05	3.921	1.163	65.14	4.201
		1.232	56.88	3.632	1.215	59.85	3.841	1.180	63.73	4.106
1.5	2.5	1.244	55.21	3.521	1.206	60.02	3.852	1.168	64.42	4.152
		1.246	54.94	3.502	1.221	58.81	3.771	1.183	63.22	4.071
					Wave propagating downward					
3	3	1.231	57.12	−3.649	1.195	61.39	−3.944	1.159	65.47	−4.223
		1.223	57.91	−3.703	1.174	63.18	−4.065	1.142	66.94	−4.321
1.5	2.5	1.243	55.31	−3.528	1.202	60.33	−3.874	1.164	64.68	−4.170
		1.234	56.13	−3.584	1.183	61.90	−3.979	1.150	65.85	−4.249

TABLE 2. The critical values of Grashof number $\widetilde{Gr}$, wavenumber $\widetilde{\alpha}$ and disturbance wave speed $\widetilde{c} = -\sigma^I/\widetilde{\alpha}$ for magneto-gravitational convection waves in oblique magnetic fields for $Gr_m = 15$, $\widetilde{\gamma} = 0°$, $Pr = 55$, $H^e = 100$ (odd-numbered lines) and $H^e = 10$ (even-numbered lines).

magnetic field responsible for the appearance of the cross-layer ponderomotive Kelvin force enhancing the instability. The wavenumber of the disturbance waves decreases, and as a result the disturbance wavelength increases. The disturbance waves also propagate quicker with the increase of the field inclination angle.

The inclination of the magnetic field in the vertical plane ($\delta \geqslant 5°$, $\widetilde{\gamma} = 0°$) changes the asymmetry in the behaviour of the Type I waves. In contrast to the normal field case, in an oblique field the upward propagating waves become unstable at the slightly smaller values of $\widetilde{Gr}$ than those for downward waves. The waves propagating upward are characterised by somewhat larger wavenumbers than those of their counterparts moving downward and their wave speeds are always smaller than those of the downward waves. These trends remain when the fluid approaches magnetic saturation and its magnetic susceptibilities are reduced.

As follows from table 2, regardless of whether the fluid is close to magnetic saturation ($\chi < \chi_*$) or not ($\chi = \chi_*$) the wave propagating upward in a thermomagnetically more sensitive ($H^e = 10$) fluid is characterised by a larger wavenumber and smaller wave speed than those of its less sensitive counterpart ($H^e = 100$). The basic flow becomes less stable with respect to this wave when H^e decreases. The trends detected for the downward waves are exactly opposite: they become more stable, longer and propagate faster as the fluid's thermo-magnetic sensitivity increases. These observations lead us to a qualitative conclusion that in an oblique field the waves propagating upward are expected to be observed experimentally first, and the faster they grow the shorter they become and the slower they propagate.

To this point the dependence of flow stability characteristics on the values of χ, χ_* and the field inclination angle δ has been investigated for the zero azimuthal field orientation angle $\widetilde{\gamma}$. To investigate the influence of the field orientation angle $\widetilde{\gamma}$ the stability results are computed for a representative value of $Gr_m = 15$. The critical parameter values for the case of a linear magnetisation law $\chi = \chi_* = 3$ are shown in figure 8 as functions of the magnetic field inclination and orientation angles. The flow is stable in the regions below the respective curves in figure 8(*a*). Therefore according to the discussion given in § 3 this type of instability occurs in

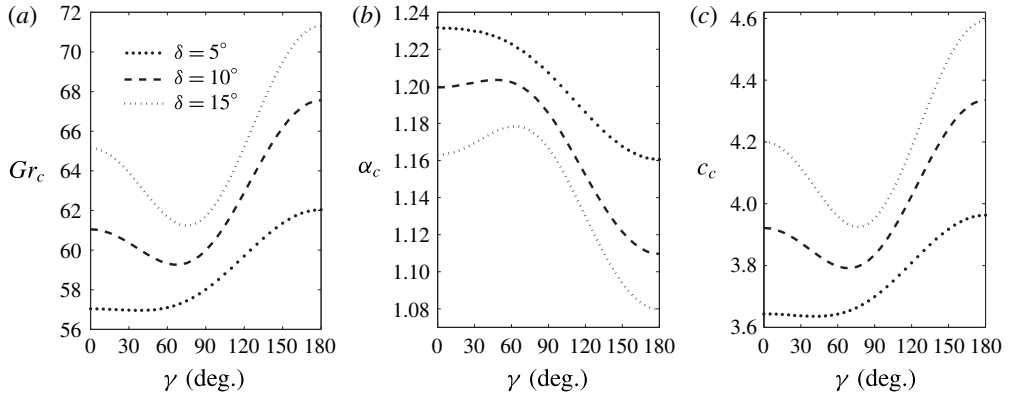

FIGURE 8. Comparison of the critical parameter values: (*a*) Grashof number Gr (the flow is stable under the respective curves), (*b*) wavenumber α and (*c*) wave speeds c as functions of the field inclination and orientation angles δ and γ for $Gr_m = 15$, $H^e = 100$, $Pr = 55$ and $\chi = \chi_* = 3$.

the form of two-dimensional patterns that are periodic in the vertical y direction with a wavenumber $\widetilde{\alpha} = \alpha$. In this case $\widetilde{\gamma} = \gamma$ and $\widetilde{Gr} = Gr$ and thus in the rest of this section the tildes are omitted. Regardless of the field orientation the basic flow becomes more stable at larger field inclination angles δ. This is primarily due to the geometric reduction of the active normal component of the applied magnetic field, which is proportional to $\cos\delta$ (see discussion in Rahman & Suslov (2015)). With the increase of the field inclination angle δ the wavenumber decreases (see figure 8*b*) so that the distance between the instability rolls increases. It follows from figure 8(*c*) that as the field inclination angle increases the wave speed also increases. The similar numerical results for a stronger magnetisable fluid with $\chi = \chi_* = 5$ remain qualitatively the same. Thus they are not presented here. However, we note that the basic convection flow of a stronger magnetisable fluid generally becomes more stable for all field orientation angles γ, and its instability patterns are characterised by a smaller wavenumber and a faster wave speed.

As seen from figure 8(*a*), the instability detected for $\gamma = 180°$ occurs at noticeably higher values of Gr_c than those for $\gamma = 0°$. This indicates that the up–down symmetry of the field influence is broken. This can be traced back to the curvature of magnetic field lines within the layer of ferrofluid discussed in Rahman & Suslov (2015). Specifically, as follows from figures 9–11 in Rahman & Suslov (2015), in the absence of the gravitational field changing the field orientation angle γ from 0° to 180° reverses the sign of the curvature of magnetic field lines. This leads to the reversal of the sign of the wave speed of thermomagnetically driven disturbances. At the same time when the gravity is taken into account, the computational data reported so far indicates that the wave propagating upward near the hot wall remains most dangerous, at least for $\delta \geqslant 5°$. Thus changing the field orientation angle γ by 180° leads to the change from the arrangement when gravitationally and thermomagnetically induced disturbances propagate in the same direction to that when they counter-propagate, and the overall instability is suppressed in the latter case.

The most prominent feature of figure 8(*a*) is the existence of the minima of the $Gr_c(\gamma)$ curves. Such minima are more pronounced in stronger magnetisable fluids characterised by the larger value of χ (not shown in the figure). Their existence

demonstrates that for each field inclination angle δ there exists a preferred field orientation angle γ that promotes the onset of magneto-gravitational instability the most.

As shown in Rahman & Suslov (2015), in zero gravity environment the most dangerous instability patterns are aligned with the in-layer component of the applied magnetic field. It is also known (Kirdyashkin *et al.* 1971) that in the absence of magnetic field (i.e. when $Gr_m = 0$) the thermo-gravitational waves arising in a large-Prandtl-number fluid consist of the horizontally uniform structures. Therefore intuitively one might expect that when both Gr and Gr_m are non-zero the least stable situation would occur when the direction of the in-layer component of the applied oblique magnetic field is horizontal, that is when $\gamma = 90^\circ$ and $H_y^e = 0$. Yet the computational results presented in figure 9(*a*) show that the field orientation angle γ_{min} for which the instability first occurs tends to 90° only for sufficiently large field inclination angles δ, that is when the in-layer component of the magnetic field becomes sufficiently large. When such a component is small ($\delta \lesssim 3.5^\circ$) the instability depends on the field orientation only weakly and the most unstable situation corresponds to $\gamma = 0^\circ$. However, for larger field inclination angles the behaviour of γ_{min} becomes a sensitive function of δ. The likely reason for such a peculiar behaviour is due to the fact reported in Rahman & Suslov (2015) for pure magnetic convection. It was demonstrated there that, similar to the gravity, an inclined magnetic field breaks a planar symmetry of the arising convection flows so that the most amplified instability patterns align with the in-layer component of the applied magnetic field (see also Groh *et al.* (2007), where a similar effect of an oblique magnetic field is discussed in the context of free-surface phenomena in magnetic fluids). Such preferentially aligned patterns remain stationary in the absence of gravity. Therefore even though the geometrical optimality might favour the alinement of the two instability patterns described above the competition between travelling thermo-gravitational waves and stationary magnetoconvection rolls would, to some degree, hinder the development of the overall instability. On the other hand, it was also shown in Rahman & Suslov (2015) that the thermo-magnetic instability patterns that are not aligned with the in-layer component of the magnetic field (i.e. observed for $\gamma \neq 90^\circ$ in the current context), while characterised by a smaller growth rate have a non-zero wave speed. Such non-stationary wave-like patterns therefore could be favoured when the magnetic instability overlaps with the vertically propagating horizontally uniform thermo-gravitational waves. Therefore the choice of $\gamma_{min} \neq 90^\circ$ appears to be due to the competition between the two optimality criteria: maximising the amplification rate of combined thermo-gravitational and thermo-magnetic instabilities and matching their propagation speeds.

It follows from figure 9(*b*) that there always exists the overall optimal orientation of magnetic field (δ_{min}, γ_{min}), which minimises the value of the critical Grashof number $Gr_{c,min}$. In particular, for $Gr_m = 15$, $\chi = \chi_* = 3$ and $Pr = 55$, $Gr_{c,min} \approx 56.16$, $\delta_{min} \approx 2^\circ$ and $\gamma_{min} = 0^\circ$. Such a global minimum corresponds to a disturbance waves with a wavenumber $\alpha_{c,min} \approx 1.234$, see figure 9(*c*). Figure 9(*d*) indicates another noteworthy feature of the wave-like instabilities detected in an oblique field: the upward propagating wave becomes the most dangerous for all optimal field orientations at $\delta \gtrsim 3.5^\circ$. For smaller field inclination angles the most unstable wave propagates downward (consistently with findings reported in table 1 for normal field) although the stability characteristics of the wave propagating upward remain very close. At larger field inclination angles the symmetry-breaking effect of a magnetic field becomes more pronounced and the switch of the dominant instability mode to

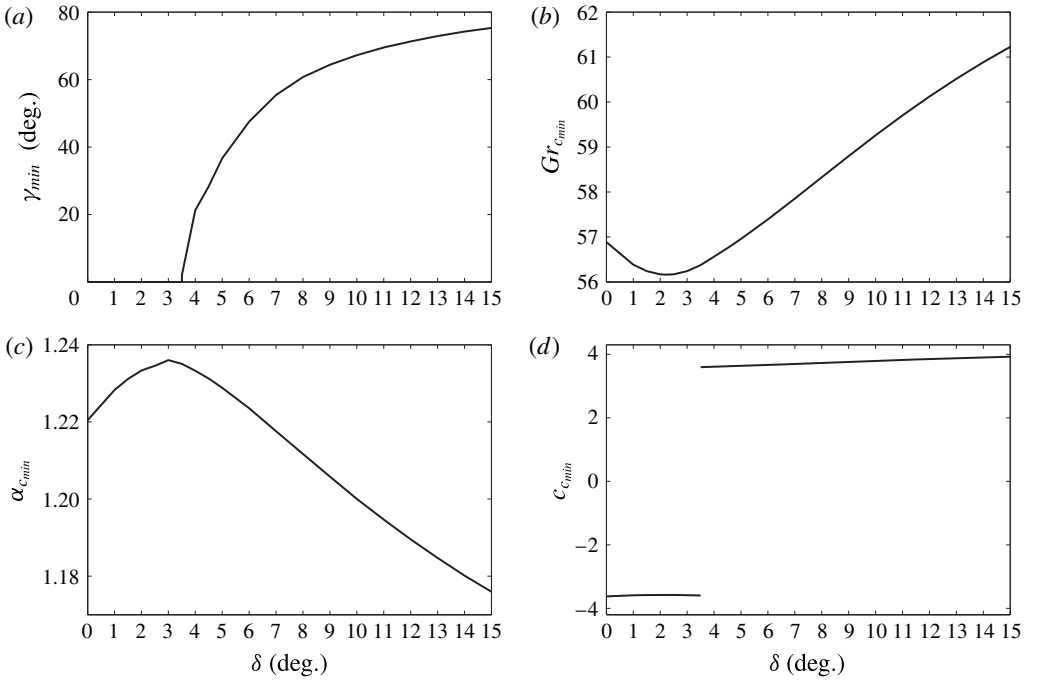

FIGURE 9. (*a*) The value of the field orientation angle γ_{min} at which the instability first occurs and (*b–d*) the corresponding critical parameters as functions of the field inclination angle δ for $Gr_m = 15$, $H^e = 100$, $Pr = 55$ and $\chi = \chi_* = 3$.

the upward propagating wave occurs, see figure 9(*d*). This switch is accompanied by the appearance of a well-defined non-zero optimal field orientation angle as seen in figure 9(*a*). The comparison of the critical parameters for the waves propagating upward and downward is presented in figure 10 for a representative field inclination angle $\delta = 5^\circ$ in a linear magnetisation regime $\chi = \chi_* = 3$. The difference between the characteristics of the two waves becomes finite but remains relatively small so that the waves are expected to co-exist in realistic experiments. Therefore the experimental ability to observe both waves is important.

Figure 10 demonstrates that the critical parameter curves for both waves have qualitatively similar shapes. The basic flow becomes unstable with respect to the upward wave for somewhat smaller values of Gr. Quantitatively, the differences between the critical parameters for the two waves are more evident for $\gamma \to 0^\circ$ or $\gamma \to 180^\circ$, that is when the applied magnetic field belongs to a vertical plane perpendicular to the fluid layer walls. For such a field orientation the wavelength of the upward propagating waves is slightly shorter than that of the downward waves.

Our computations (not shown here) confirm that when the fluid approaches magnetic saturation (i.e. both χ and χ_* decrease and become unequal) qualitatively the critical parameter curves for the wave-like disturbances remain similar to those seen in figure 10. However, the values of both the critical Grashof number and the optimal field orientation angle γ decrease (e.g. from $Gr_c \approx 56.96$ and $\gamma \approx 38^\circ$ at $\chi = \chi_* = 3$ to $Gr_c \approx 55.15$ $\gamma \approx 35^\circ$ at $\chi = 1.5$ and $\chi_* = 2.5$).

In conclusion of this section we compare the stability characteristics of the basic flow with respect to wave-like disturbances of Type I for thermomagnetically less

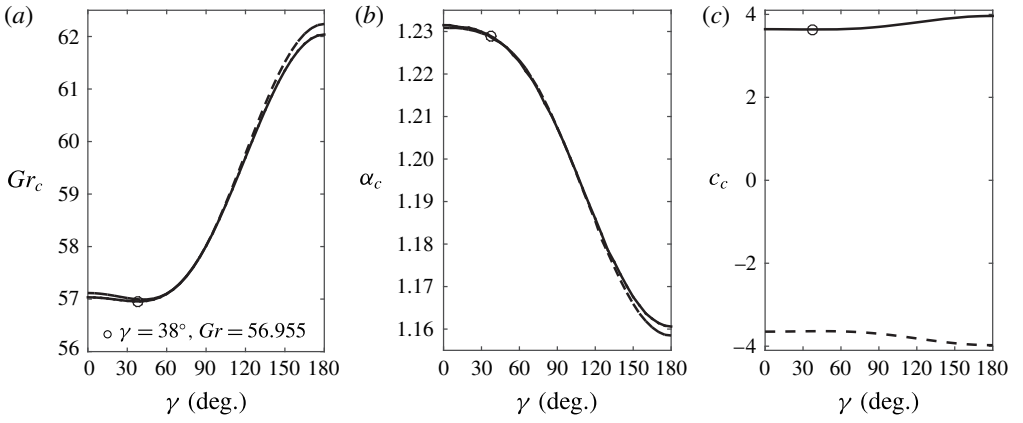

FIGURE 10. Comparison of the critical parameter values for the waves propagating upward (solid line) and downward (dashed line): (*a*) Grashof number Gr (the flow is stable under the respective curves), (*b*) wavenumber α and (*c*) wave speeds c as functions of the azimuthal angle γ for $Gr_m = 15$, $H^e = 100$, $Pr = 55$, $\delta = 5°$ and $\chi = \chi_* = 3$.

($H^e = 100$) and more ($H^e = 10$) sensitive fluids, see figure 11. The waves propagating upward remain the most dangerous in both types of fluids, so only the critical parameters corresponding to them are shown. There are a number of general trends that are evident from figure 11. Firstly, the flows of thermomagnetically more sensitive fluids placed in a magnetic field with a predominantly vertical in-layer component (γ close to 0 or 180°) are generally less stable than those of their less sensitive counterparts. When the applied oblique magnetic field is mostly horizontal ($\gamma \sim 90°$), that is when the curvature of the magnetic field lines within the fluid layer (Rahman & Suslov 2015) is in the plane perpendicular to the direction of the gravity, the magnetic sensitivity of a fluid does not appear to play a significant role in defining the flow stability parameters. Secondly, the wave-like instability patterns arising in a more thermomagnetically sensitive fluid are characterised by a larger wavenumber and thus by convection structures that are closer packed in the direction of the gravity when $\gamma > 90°$, once again demonstrating the symmetry-breaking effect of an oblique magnetic field. Thirdly, the instability waves arising in a thermomagnetically more sensitive fluid generally have a somewhat smaller wave speed. Therefore increasing the fluid's thermo-magnetic sensitivity quenches the propagation of disturbance waves. This is consistent with the findings reported in Rahman & Suslov (2015) that the most amplified thermomagnetically driven instability patterns remain stationary in the absence of gravity. The computational data (not shown) also demonstrate that these trends are not affected when the fluid approaches its magnetic saturation with $\chi < \chi_*$.

4.4. *Stability diagrams for an equivalent two-dimensional problem*

In § 4.3 the flow instability properties associated with the wave-like Type I disturbances have been discussed in detail. The goal of this section is to identify parametric regions where different physical mechanisms lead to the onset of instability in the considered geometry. To do that the representative complete stability diagrams for an equivalent two-dimensional problem have been computed and presented in figure 12.

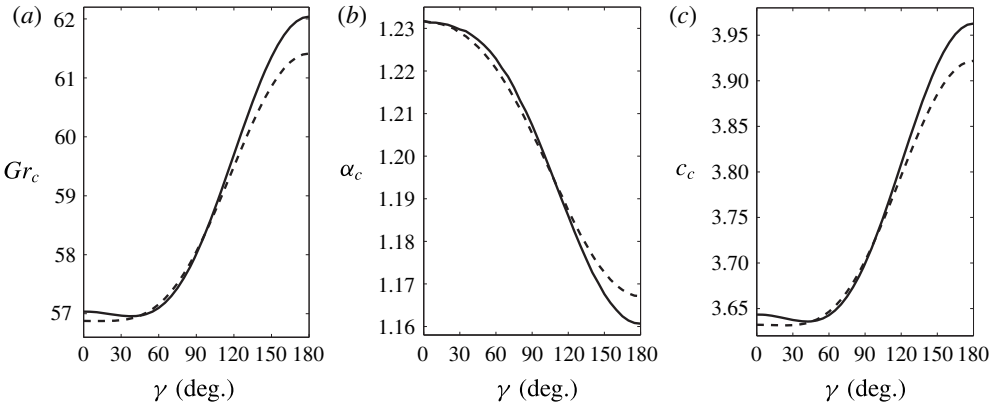

FIGURE 11. Comparison of the critical parameter values for thermomagnetically less ($H^e = 100$, solid line) and more ($H^e = 10$, dashed line) sensitive fluids: (*a*) Grashof number Gr (the flow is stable under the respective curves), (*b*) wavenumber α and (*c*) wave speeds c as functions of the azimuthal angle γ for $Gr_m = 15$, $Pr = 55$, $\delta = 5^\circ$ and $\chi = \chi_* = 3$. Type I instability.

4.4.1. *Normal field*

We start with the discussion of a typical stability diagram for a normal magnetic field shown in figure 12(*a–c*). While computed for different values of Prandtl number and magnetic susceptibilities, qualitatively, this diagram is similar to that given in figure 2 for $Pr = 130$ in Suslov (2008). This demonstrates that the dependence of the flow stability characteristics on thermo-viscous properties of the fluid placed in the normal magnetic field and on its magnetic susceptibilities is just quantitative.

The stability diagram consists of three lines each representing a different type of instability characterised by its own wavenumber as follows from figure 12(*b*). The solid line in figure 12(*a*) starts from $Gr_m = 0$, which corresponds to the threshold of a classical thermo-gravitational convection instability (Kirdyashkin *et al.* 1971; Chait & Korpela 1989; Gershuni *et al.* 1989; Wakitani 1996). As discussed earlier, this is the Type I instability characterised by two counter-propagating waves. The basic flow is subject to such an instability above the solid line in figure 12(*a*). Therefore as discussed in § 3 the Type I instability corresponds to vertically propagating patterns with $\alpha = \widetilde{\alpha}$ and $\beta = 0$ that are y-periodic and uniform in the horizontal z-direction. Recollect that in this case $\widetilde{\gamma} = \gamma$.

The dashed line in figure 12(*a*) starts from $\widetilde{Gr} = 0$ and therefore corresponds to the threshold of magnetoconvection. In this case, the disturbance amplification rate σ^R is real (see figure 2*b*,*e*). As follows from an earlier discussion, this is the Type II instability that is stationary in the normal field (see also Finlayson (1970), Belyaev & Smorodin (2010)). The basic flow is unstable below the dashed line in figure 12(*a*) and therefore an additional analysis of the inverse Squire's transformation is required to determine the spatial orientation of such patterns. To perform it refer to figure 13(*a*), where the linear amplification rate σ^R is plotted as the function of the Squire-transformed ('two-dimensional') Grashof number $\widetilde{Gr}$ (see relationships (3.7)). The maximum amplification rate of the Type II instability (the dashed line) is detected when $\widetilde{Gr} \to 0$. The inverse Squire's transformation then states that the disturbance amplification rate of three-dimensional perturbations, which is invariant

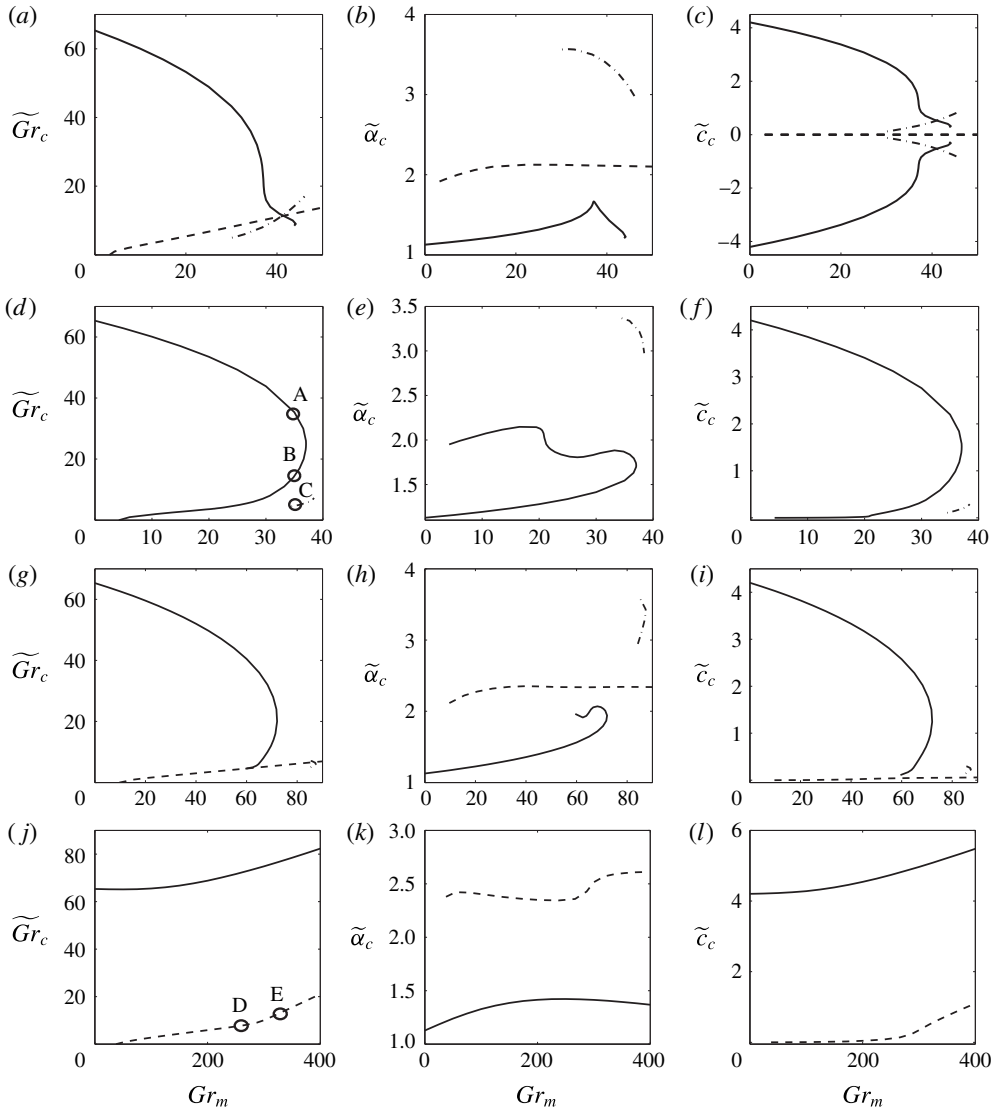

FIGURE 12. Variation of stability diagrams (*a*,*d*,*g*,*j*), wavenumbers (*b*,*e*,*h*,*k*) and wave speeds (*c*,*f*,*i*,*l*) with the magnetic field inclination for $H^e = 100$, $Pr = 55$, $\chi = \chi_* = 3$, $\widetilde{\gamma} = 0°$ and (*a–c*) $\delta = 0°$, (*d–f*) $\delta = 5°$, (*g–i*) $\delta = 10°$ and (*j–l*) $\delta = 15°$.

under Squire's transformation, will be observed at any value of a non-transformed ('three-dimensional') Grashof number Gr related to $\widetilde{Gr}$ as

$$\alpha Gr = \sqrt{\alpha^2 + \beta^2}\widetilde{Gr}. \tag{4.2}$$

This means that the maximum amplification rate observed for the Type II instability when $\widetilde{Gr} \to 0$ will be observed at an arbitrary value of the non-transformed Grashof number Gr provided that $\alpha \to 0$. That is $\beta \to \widetilde{\alpha}$, where $\widetilde{\alpha}$ is the left-most value along the dashed line in figure 13(*b*). In other words, the Type II instability in the form of

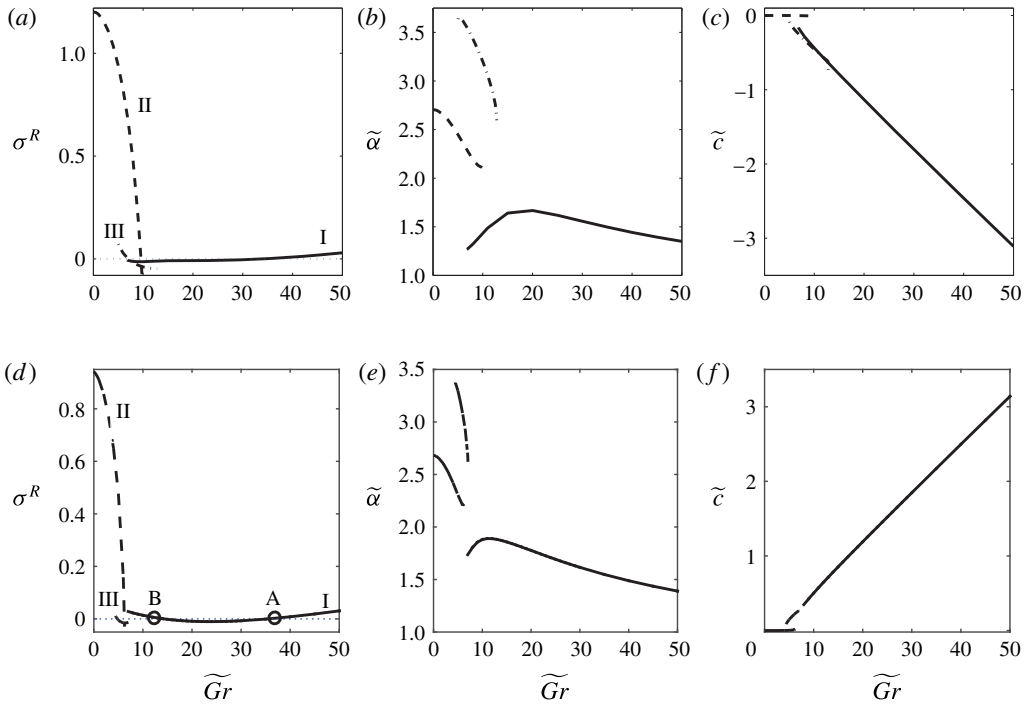

FIGURE 13. (*a*,*d*) Maximum amplification rate for an equivalent two-dimensional problem; (*b*,*e*) the corresponding wave numbers $\widetilde{\alpha}$ and (*c*,*f*) wave speeds for $Gr_m = 35$, $H^e = 100$, $Pr = 55$ and $\chi = \chi_* = 3$ in normal ((*a*–*c*), $\delta = 0°$) and oblique ((*d*–*f*), $\delta = 5°$, $\widetilde{\gamma} = 0°$) magnetic fields.

vertical magnetoconvection rolls (so that $\gamma = \widetilde{\gamma} + 90°$ for this instability mode) will arise for arbitrary values of Gr once Gr_m exceeds the critical value corresponding to the left-most point along the dashed line in figure 12(*a*). For any values of Gr exceeding those corresponding to the solid line in figure 12(*a*) the stationary vertical rolls of the Type II instability will overlap with the vertically propagating Type I instability waves.

Given that the inverse Squire's transformation indicates that for sufficiently large values of Gr_m the flow is always unstable with respect to vertical thermo-magnetic rolls regardless of the value of Gr the physical meaning of the dashed line in figure 12(*a*) needs to be clarified. When the gravity is absent and $Gr = 0$ the arising magnetoconvection rolls can be arbitrarily oriented as all directions in the fluid layer plane are equivalent. When the gravity is introduced and Gr becomes non-zero the basic gravitational convection flow arises and removes the spatial degeneracy so that the vertically oriented rolls are preferred. Yet it is clear that at small values of Gr rolls of all other orientations still can exist even though vertical rolls now have a larger growth rate. As the value of the Grashof number increases, the growth rate of the vertical rolls remains the same at fixed Gr_m, but the growth rate of non-vertical rolls becomes smaller. Eventually, when the value corresponding to the dashed line in figure 12(*a*) is reached, horizontal rolls cannot grow anymore and disappear. Above the dashed line there exists a maximum roll inclination angle beyond which the Type II instability cannot be observed. To clarify this consider the following example. Computations show that in the normally applied field the

flow stabilisation occurs when the value of the Squire-transformed Grashof number $\widetilde{Gr}$ exceeds 9.55 for $Gr_m = 35$ and $\chi = \chi_* = 3$ (this corresponds to the point in figure 13(*a*) where the dashed line crosses zero and to the respective critical point $(Gr_{mc}, \widetilde{Gr}_c) = (35, 9.55)$ on the dashed line in figure 12*a*). Say, the experimental value of interest is $Gr = 15$. Then we conclude that in such experimental conditions it is expected that the instability patterns will be in the form of stationary vertical rolls that however could be modulated by weaker rolls with the axes forming the angle of up to

$$\sin^{-1}\frac{\alpha}{\widetilde{\alpha}_c} = \sin^{-1}\frac{\widetilde{Gr}_c}{Gr} = \sin^{-1}\frac{9.55}{15} \approx 40^\circ, \tag{4.3}$$

with the vertical y-direction. The larger the experimental value of Gr is the smaller the allowed modulation angle becomes. This has a straightforward physical explanation: the increase in the value of Grashof number intensifies the vertical basic flow velocity (see (3.1)), which in turn results in a stronger vertical alignment of the instability patterns.

The Type III instability boundary is shown in figure 12(*a*) by the dash-dotted line. The basic flow is stable with respect to this mode below it. As seen from figure 12(*b*), the corresponding instability patterns have larger wavenumbers (dash-dotted line) than those of the Type I and Type II instabilities (solid and dashed lines, respectively). As follows from figure 12(*c*), similar to the Type I instability, the Type III instability arises in the form of two waves counter-propagating with speeds that become faster than those of the Type I waves for sufficiently large values of Gr_m. The peculiar feature of the Type III instability seen in figure 12(*a*) is that its boundary appears to end abruptly at certain values of gravitational and magnetic Grashof numbers (this feature is also observed at small non-zero field inclination angles, see point C in figure 12*d*). Such an unusual behaviour was discussed in detail in Suslov (2008). There it was shown that the Type III instability appears as a result of a sudden qualitative change in the problem's dispersion relation when its branches corresponding to either the Type I or Type II instabilities bifurcate resulting in the appearance of the Type III waves. Experimentally, the appearance of the Type III instability could be detected either by observing a sudden transition from stationary (Type II) to non-stationary (Type III) patterns at relatively small values of $\widetilde{Gr}$ or from one unsteady pattern (Type I) to another (Type III) with a shorter wavelength.

Another feature distinguishing the Type III instability from its Type I and Type II counterparts, whose patterns are characterised by a fixed spatial orientation, is that the main periodicity direction for the Type III instability depends on the value of the Grashof number. For example, as follows from figure 13(*a*) for $Gr_m = 35$ the Type III instability has the largest growth rate at $\widetilde{Gr}_c = 5.07$ (the left end of the dash-dotted line) where it has the form of vertically propagating waves with $\alpha = \widetilde{\alpha} \approx 3.636$ and $\beta = 0$. However according to the inverse Squire's transformation, for any larger value of the Grashof number it will be seen as a pair of oblique waves counter-propagating along the direction forming the angle $\cos^{-1}(\widetilde{Gr}_c/Gr)$ with the vertical y direction. In other words, as the Grashof number (and thus the vertical basic flow velocity) increases the axes of the Type III instability rolls approach the vertical, and the patterns drift almost horizontally. At the same time, the Type I instability patterns remain horizontal and propagate vertically. For example, at $Gr = 15$ the Type III instability waves are expected to propagate along the direction forming the angle

of $\cos^{-1}(5.07/15) \approx 70^\circ$ with the vertical direction rather than vertically and their spanwise direction is expected to form the angle of $\sin^{-1}(5.07/15) \approx 20^\circ$ with the vertical.

4.4.2. *Field inclined in the plane containing the main periodicity direction ($\widetilde{\gamma} = 0^\circ$)*

The magnetic field inclination adds further complexity to the already quite complicated instability picture in the presence of both gravitational and magnetic effects. The stability diagram for an oblique magnetic field ($\delta = 5^\circ$, $\widetilde{\gamma} = 0^\circ$) is shown in figure 12(*d*). The comparison with figure 12(*a*) for a normal field shows that the flow stability region becomes larger in an oblique magnetic field. This is consistent with the numerical results given in tables 1 and 2. As follows from figure 12(*e*), similar to the normal field case the Type I instability is characterised by a smaller wavenumber (the solid line) compared to that of the Type III instability (the dash-dotted line). However the symmetry of the disturbance thermal waves propagation is broken in an oblique field and the upward wave becomes more dangerous. Therefore in figure 12(*f*) only the critical wave speed for this wave is shown. It increases monotonically with Gr_m.

It is remarkable that the qualitative change in stability diagram occurs even for such small field inclination angles. The solid and dashed stability boundary lines distinguished in figure 12(*a*) merge in figure 12(*d*) indicating that the distinction between the Type I and Type II instabilities becomes blurred when the applied magnetic field is inclined in a plane containing the periodicity direction. The dash-dotted line in the lower right corner in figure 12(*a*) becomes much shorter meaning that the Type III instability could be hard to detect experimentally in an oblique field. Even though the solid line originates from $\widetilde{Gr} = 0$ in figure 12(*d*), it corresponds to non-stationary magnetoconvection, see the lower part of the solid curve in figure 12(*f*). This is consistent with the results presented in Rahman & Suslov (2015) where it has been shown that the thermo-magnetic instability patterns that are not aligned with the in-layer component of the applied magnetic field are always non-stationary.

While the orientation of the Types II and III instability patterns remains qualitatively unaffected by the small field inclination, the qualitative changes occur in the orientation of the Type I instability patterns at sufficiently large values of Gr_m. As seen from figure 13(*d*), the $\sigma^R(\widetilde{Gr})$ curve crosses the zero level twice at points A and B (see also the corresponding points in figure 12*d*). According to the inverse Squire's transformation the decreasing segment of the $\sigma^R(\widetilde{Gr})$ curve to the left of point B in figure 13(*d*) indicates the existence of oblique instability structures with the orientation depending on the value of Gr. For the relatively small values of $Gr < Gr_B$ the fastest growing Type I instability pattern is almost horizontal with $\beta = 0$, but as Gr increases the most unstable patterns turn and approach vertical (β increases at the expense of α). This continues until Gr reaches the value of Gr_A. At this point another pair of the Type I waves appears that are horizontally uniform ($\beta = 0$) and propagate vertically. Figure 13(*c*,*f*) also confirms the conclusion made earlier that due to the symmetry-breaking effect of nonlinear fluid magnetisation the most dangerous Type I pattern switches from the wave propagating downward in a normal field to the one propagating upward in an oblique field. However the growth rates of both waves remain close so that a counter-propagating wave pair is likely to be seen in experiments. Figure 13(*a*,*d*) also demonstrates that for the sufficiently large values of Gr_m the Type II instability has a much larger growth rate than those of the

Type I and Type III patterns. Therefore stationary vertical thermo-magnetic rolls are expected to dominate the overall disturbed flow. Yet the presence of the Type I and III instabilities should be visible experimentally as non-stationary three-dimensional modulations of vertical rolls, which has indeed been detected in experiments reported in Suslov *et al.* (2010, 2012).

The magnetic field inclination continues to play a very important role in shaping the parametric stability boundaries of the considered flow when δ is increased further. The stability diagram for $\delta = 10^\circ$ and $\widetilde{\gamma} = 0^\circ$ shown in figure 12(*g*) demonstrates that a significant stabilisation of the flow with respect to the Type I disturbances is observed (the area bounded by the solid line increases). The Type I and Type II instabilities are again easily distinguished. The waves propagating upward still remain the most dangerous for the non-zero values of the magnetic Grashof number.

At even larger field inclination angles another qualitative change occurs. As seen from figure 12(*j*), for $\delta = 15^\circ$ the Type III instability is not detected over the investigated range of the governing parameters. The critical values of $\widetilde{Gr}$ for the Type I instability now increase monotonically with Gr_m. This is traced back to the aligning influence of the applied magnetic field. With the increasing field inclination angle δ and $\widetilde{\gamma} = \gamma = 0^\circ$ the vertical in-layer field component increases as well and so does its 'pattern aligning' effect. Thus the vertically propagating and horizontally uniform Type I waves are suppressed by the inclined field applied in a vertical plane and require a much stronger gravitational buoyancy characterised by $\widetilde{Gr}$ to arise. The Type II instability characteristics presented for the field inclined at $\delta = 15^\circ$ and shown in figure 12(*j–l*) change in a peculiar manner. For small values of the magnetic Grashof number the Type II instability boundary (the basic flow is unstable below the dashed line) rises almost linearly and the critical wavenumber remains almost constant at $\widetilde{\alpha} \approx 2.5$. This instability remains nearly stationary up to $Gr_m \sim 300$ (e.g. point D in figure 12*j*). However for larger values of Gr_m the slope of the stability boundary changes rapidly (even though in a continuous manner) to a larger value, (e.g. point E in figure 12*j*) and so does the value of $\widetilde{\alpha}$. The critical wave speed becomes non-zero and starts growing.

In conclusion of this section we note that our computations not discussed here in detail show that the main effect of the approaching magnetisation saturation regime $\chi < \chi_*$ is the disappearance of the Type III instability even at the field inclination angles as small as $\delta = 5^\circ$. However, the Types I and II instabilities remain qualitatively unchanged. Thus no detailed discussion of magnetic saturation regimes will be given here. We have also explored the influence of the fluid's thermo-magnetic sensitivity on the stability characteristics of the flow by computing the results for $H^e = 10$. Again it was found that the only qualitative effect the variation of this parameter leads to is the disappearance of the Type III instability in a more magnetically sensitive fluid. Therefore the specific results presented in this section appear to be robust. They provide a sufficiently complete view of the instability processes taking place in the considered geometry for a wide range of physical conditions.

4.4.3. *Arbitrary field orientation*

All stability diagrams discussed so far have been computed for $\widetilde{\gamma} = 0^\circ$. It is of interest now to compare the flow stability characteristics in the applied fields of different orientations. This is done in figure 14 for $\delta = 10^\circ$. The figure demonstrates a sensitive dependence on the choice of $\widetilde{\gamma}$. However this variation is not monotonic. As $\widetilde{\gamma}$ increases from 0°, the parametric stability region in figure 14(*a*) initially shrinks

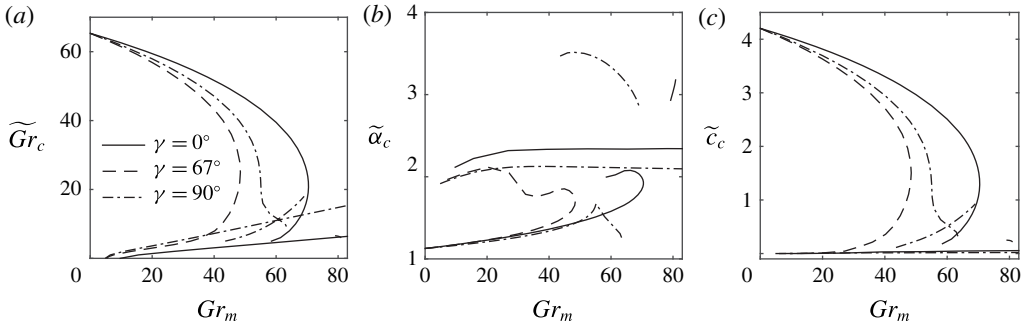

FIGURE 14. Comparison of the critical values for $H^e = 100$, $Pr = 55$, $\chi = \chi_* = 3$, $\delta = 10°$ and various field orientation angles $\widetilde{\gamma}$: (*a*) stability diagram for an equivalent two-dimensional problem; (*b*) critical wavenumber $\widetilde{\alpha}_c$ and (*c*) the corresponding wave speeds along the stability boundaries shown in plot (*a*).

and then starts growing. Therefore the general conclusion is that there exists an optimal field orientation angle $\widetilde{\gamma}$ for which the basic flow becomes most unstable. The existence of the optimal field orientation angle γ_{min} for the Type I instability has been discussed in detail in § 4.3 and here we will focus on the Type II instability.

The most unstable pattern of the Type II instability corresponds to vertical rolls with $\alpha = 0$ and $\beta = \widetilde{\alpha}$. However rolls of all other orientations can also exist up to $Gr = \widetilde{Gr}_c$ corresponding to the values shown in figure 15(*a*) (computed for $Gr_m = 15$ as an example). The vertical alinement of instability patterns occurs for the larger values of Gr. The value of $\widetilde{Gr}_c$ depends on the field orientation angle $\widetilde{\gamma}$. As follows from figure 15(*a*), such an alignment for $Gr_m = 15$ and $\delta = 5°$ is most delayed when the field is oriented at the angle $\gamma = 90° \pm \widetilde{\gamma} \approx 237°$ or $-57°$ to the vertical y axis. Figure 15(*b*) demonstrates that the orientation of the applied magnetic field also affects the wavelength of the Type II instability patterns: it slightly increases as the field orientation angle approaches the optimal value. As follows from figure 15(*c*) the Type II instability in this example remains essentially stationary for all field orientation angles (this, however, is not the case for larger values of Gr_m, as seen from figure 12*f*).

For the larger values of Gr_m the dependence of the critical values on the field orientation angle $\widetilde{\gamma}$ becomes more complicated. As seen from figure 16 unlike for smaller values of Gr_m both the Type II (dashed line) and Type I (solid line) instabilities can be detected when varying $\widetilde{\gamma}$. The two types of instabilities here are distinguished by the values of their wavenumbers (the Type I instability has a longer wavelength, see figure 16*b*) and wave speeds (the Type I instability is wave-like while the Type II patterns are virtually stationary, see figure 16*c*). Both instabilities have their own optimal field orientation angles (shown by symbols). Namely, as follows from the inverse Squire's transformation discussed earlier, for the representative value of $Gr_m = 35$ the vertical alignment of the Type II instability patterns is delayed the most (up to $Gr \approx 9.142$) if the field is oriented at $\gamma = 90° \pm \widetilde{\gamma} \approx 241°$ or $-61°$. At the same time such a delay (up to $Gr \approx 15.023$) in the vertical alignment of the Type I instability patterns is most evident for the field orientation angles in the range $0° < \widetilde{\gamma} < 90°$ (see the maximum of the solid curve marked by the square in figure 16*a*). Therefore we conclude that the orientation of the applied magnetic field can have a profound influence on the type of the observed convection patterns,

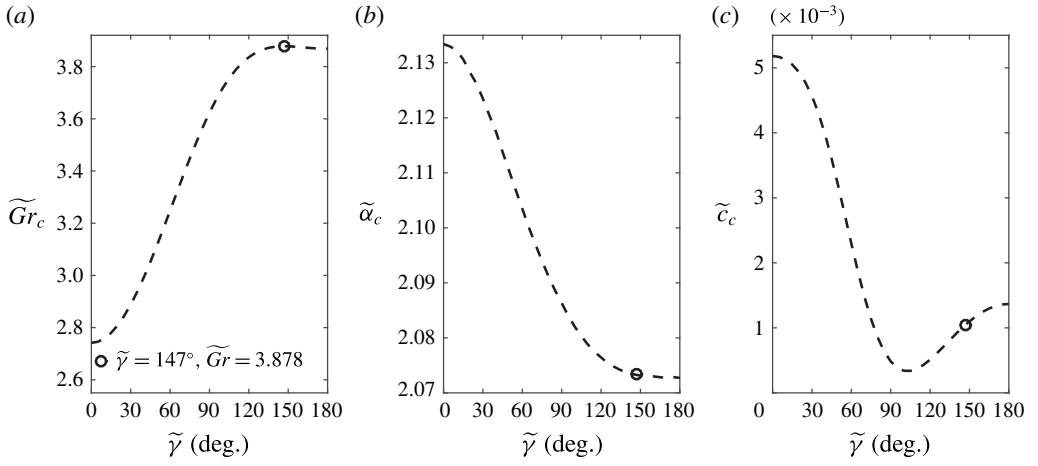

FIGURE 15. The critical parameter values: (*a*) Grashof number $\widetilde{Gr}$ (the flow is stable above the curve), (*b*) wavenumber $\widetilde{\alpha}$ and (*c*) wave speeds $\widetilde{c}$ as functions of the field orientation angle $\widetilde{\gamma}$ for $\delta = 5°$, $Gr_m = 15$, $H^e = 100$, $Pr = 55$ and $\chi = \chi_* = 3$.

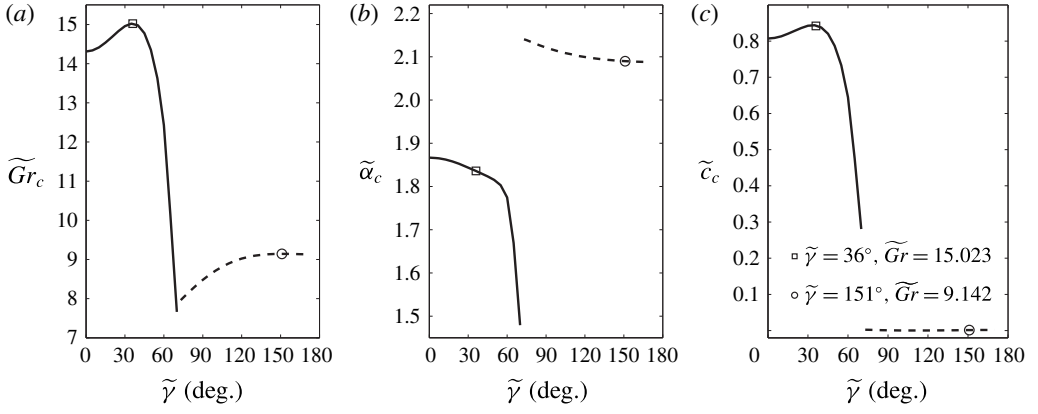

FIGURE 16. Same as figure 15 but for $Gr_m = 35$.

which indeed has been observed near the edges of the ferrofluid layer, where the field inclination is essential and unavoidable, in experiments reported in Suslov *et al.* (2010, 2012).

5. Conclusions

The linear stability of the base convection flow in a vertical differentially heated layer of ferrofluid placed in an oblique magnetic field was investigated. The essentially three-dimensional original problem was cast in an equivalent two-dimensional form using Squire's transformation to reduce computational cost. Subsequently, a full three-dimensional dynamics was recovered using the inverse Squire's transformations. The characteristics of all instability modes were investigated as functions of the inclination and orientation angles and the magnitude of the applied magnetic field for various values of magnetic parameters and for linear and nonlinear magnetisation laws.

It has been shown that two distinct mechanisms, thermo-gravitational (buoyancy-driven) and thermo-magnetic, acting simultaneously are responsible for the appearance of various instability modes. Three main types of instability patterns corresponding to thermo-gravitational, thermo-magnetic and magneto-gravitational convection are found to exist. A thermo-magnetic convection is caused by the variation of the fluid magnetisation and magnetic field across the non-uniformly heated layer, while a magneto-gravitational convection instability arises due to the combined action of the gravitational and magnetic buoyancy. It has been shown that in the magneto-gravitational instability regime two waves propagate inside the layer: up near the hot wall and down near the cold one. The upward propagating wave becomes more dangerous when the field inclination angle becomes larger than 3°–5°. The comparison of the up and downward propagating waves shows that the former is characterised by a slightly lager critical wavenumber.

The basic flow becomes generally more stable and the disturbance waves propagate quicker when the field inclination angle increases. The stability characteristics of the basic flow with respect to wave-like disturbances have been compared for thermomagnetically less ($H^e = 100$) and more ($H^e = 10$) sensitive fluids, and it has been found that the upward propagating wave remains the most dangerous in both types of fluids. It is established that for each field inclination angle there exists a preferred field orientation angle that promotes the onset of magneto-gravitational instability the most. While for a thermo-magnetic instability at very small values of the gravitational Grashof number the field inclined in a vertical plane is found to promote the instability the most, for other types of instability the optimal field orientation depends on the choice of the governing physical parameters.

It is also demonstrated that the inclination of the external magnetic field breaks the cross-layer flow symmetry and leads to the preferential shift of instability structures toward the hot wall, which is more pronounced in magnetically more sensitive fluids characterised by a smaller non-dimensional magnetic field magnitude.

Acknowledgements

The authors would like to thank Professor A. A. Bozhko and Mr A. S. Sidorov of the Physics Department at Perm State University, Russia for discussing the relevance of the presented computational results to the experimental studies currently conducted in their group.

REFERENCES

BASHTOVOY, V. G., BERKOVSKY, B. M. & VISLOVICH, A. N. 1988 *Introduction to Thermomechanics of Magnetic Fluids*. Hemisphere.

BATCHELOR, G. K. 1954 Heat transfer by free convection across a closed cavity between vertical boundaries at different temperatures. *Q. Appl. Maths.* **12**, 209–233.

BELYAEV, A. V. & SMORODIN, B. L. 2010 The stability of ferrofluid flow in a vertical layer subject to lateral heating and horizontal magnetic field. *J. Magn. Magn. Mater.* **322**, 2596–2606.

BLUMS, E. YA., MAIOROV, M. M. & TSEBERS, A. O. 1989 *Magnetic Fluids*. Zinatne, Riga, Latvia (in Russian).

BOZHKO, A. A. & PUTIN, G. F. 1991 Experimental investigation of thermo-magnetic convection in uniform external field. *Bull. Acad. Sci. USSR* **55**, 1149–1156.

BOZHKO, A. A. & PUTIN, G. F. 2003 Heat transfer and flow patterns in ferrofluid convection. *Magnetohydrodynamics* **39**, 147–169.

BOZHKO, A. A., PUTIN, G. F., SIDOROV, A. S. & SUSLOV, S. A. 2013 Convection in a vertical layer of stratified magnetic fluid. *Magnetohydrodynamics* **49**, 143–152.

CHAIT, A. & KORPELA, S. A. 1989 The secondary flow and its stability for natural convection in a tall vertical enclosure. *J. Fluid Mech.* **200**, 189–216.

CHARLES, S. W. 2002 *The Preparation of Magnetic Fluids*, vol. 594, pp. 3–18. Springer.

FINLAYSON, B. A. 1970 Convective instability of ferromagnetic fluids. *J. Fluid Mech.* **40**, 753–767.

GERSHUNI, G. Z. & ZHUKHOVITSKY, E. M. 1953 On the stability of plane convective motion of a fluid. *Zh. Tekh. Fiz* **23**, 1838–1844.

GERSHUNI, G. Z., ZHUKHOVITSKY, E. M. & NEPOMNIASCHY, A. A. 1989 *Stability of Convective Flows*. Science, Moscow, Russia, (in Russian).

GOLLWITZER, C., SPYROPOULOS, A. N., PAPATHANASIOU, A. G., BOUDOUVIS, A. G. & RICHTER, R. 2009 The normal field instability under side-wall effects: comparison of experiments and computations. *New J. Phys.* **11**, 053016.

GROH, CH., RICHTER, R., REHBERG, I. & BUSSE, F. H. 2007 Reorientation of a hexagonal pattern under broken symmetry: The hexagon flip. *Phys. Rev.* E **76**, 055301.

HENNENBERG, M., WESSOW, B., SLAVTCHEV, S., DESAIVE, TH. & SCHEILD, B. 2006 Steady flows of laterally heated ferrofluid layer: influence of inclined strong magnetic field and gravity level. *Phys. Fluids* **18**, 093602.

KIRDYASHKIN, A. G., LEONT'EV, A. I. & MUKHINA, N. V. 1971 Stability of a laminar flow of fluid in vertical layers with free convection. *Fluid Dyn.* **6**, 884–888.

MUKHOPADHYAY, A., GANGULY, R., SEN, S. & PURI, I. K. 2005 A scaling analysis to characterize thermomagnetic convection. *Intl J. Heat Mass Transfer* **48**, 3485–3492.

ODENBACH, S. 1995 Microgravity experiments on thermomagnetic convection in magnetic fluids. *J. Magn. Magn. Mater.* **149**, 155–157.

ODENBACH, S. 2002 *Ferrofluids: Magnetically Controllable Fluids and Their Applications*. Springer.

PSHENICHNIKOV, A. F. & IVANOV, A. S. 2012 Magnetophoresis of particles and aggregates in concentrated magnetic fluids. *Phys. Rev.* E **86**, 051401.

RAHMAN, H. & SUSLOV, S. A. 2015 Thermomagnetic convection in a layer of ferrofluid placed in a uniform oblique external magnetic fluid. *J. Fluid Mech.* **764**, 316–348.

REIMANN, B., RICHTER, R., KNIELING, H., FRIEDRICHS, R. & REHBERG, I. 2005 Hexagons become the secondary pattern if symmetry is broken. *Phys. Rev.* E **71**, 055202.

ROSENSWEIG, R. E. 1985 *Ferrohydrodynamics*. Cambridge University Press.

SHLIOMIS, M. I. & SMORODIN, B. L. 2002 Convective instability of magnetized ferrofluids. *J. Magn. Magn. Mater.* **252**, 197–202.

SIDOROV, A. S. 2016 The influence of an oblique magnetic field on convection in a vertical layer of magnetic flud. *Mygnetohydrodynamics* **52** (to appear).

SPRENGER, L., LANGE, A., ZUBAREV, A. YU. & ODENBACH, S. 2015 Experimental, numerical, and theoretical investigation on the concentration-dependent Soret effect in magnetic fluids. *Phys. Fluids* **27**, 022001.

SUSLOV, S. A. 2008 Thermo-magnetic convection in a vertical layer of ferromagnetic fluid. *Phys. Fluids* **20** (8), 084101.

SUSLOV, S. A., BOZHKO, A. A., PUTIN, G. F. & SIDOROV, A. S. 2010 Interaction of gravitational and magnetic mechanisms of convection in a vertical layer of a magnetic fluid. *Phys. Procedia* **9**, 167–170.

SUSLOV, S. A., BOZHKO, A. A., SIDOROV, A. S. & PUTIN, G. F. 2012 Thermomagnetic convective flows in a vertical layer of ferrocolloid: Perturbation energy analysis and experimental study. *Phys. Rev.* E **86**, 016301.

SUSLOV, S. A. & PAOLUCCI, S. 1995 Stability of natural convection flow in a tall vertical enclosure under non-Boussinesq conditions. *Intl J. Heat Mass Transfer* **38**, 2143–2157.

WAKITANI, S. 1996 Formation of cells in natural convection in a vertical slot at large Prandtl number. *J. Fluid Mech.* **314**, 299–314.

ZABLOTSKY, D., MEZULIS, A. & BLUMS, E. 2009 Surface cooling based on thermomagnetic convection: numerical simulation and experiment. *Intl J. Heat Mass Transfer* **52**, 5302–5308.